NTNU – Trondheim
Norwegian University of
Science and Technology

Performance of supported catalysts for water electrolysis

Stian Gurrik

Materials Science and Engineering
Submission date: June 2012
Supervisor: Svein Sunde, IMTE

Norwegian University of Science and Technology
Department of Materials Science and Engineering

Preface

This report is a master thesis written in the spring 2012, during the last semester of the M.Sc. program: Materials Science and Engineering at NTNU, Department of Materials Science and Engineering. The work have been done in collaboration with researchers at Sintef Materials and Chemistry, and continues on a path set by NEXPEL (Next Generation PEM Electrolyzer for Sustainable Hydrogen Production), a collaboration project led by Sintef. This work takes a closer look at the catalytic activity and stability of supported oxygen evolution catalysts, with the ultimate motivation of finding a standardized and practical way of both defining and measuring the stability of an oxygen evolution catalyst.

Special thanks goes to my supervisors, Prof. Svein Sunde and Magnus Thomassen, for guidance. I would also like to thank Luis Colmenares and Edel Sheridan for their contributions to the experimental work.

The work described in this thesis has been done individually and in accordance with NTNU regulations.

Stian Gurrik

Tronheim, June 14, 2012.

Sammendrag

Den mest aktive katalysatoren for oksygenutvikling i PEM vannelektrolyse er ruteniumoksid. Som kommersiell katalysator er den store ulempen dårlig stabilitet. Hvis rutenium blandes med iridium øker stabiliteten, men det ville vært gunstig å finne en rimeligere erstatning til iridium. I dette arbeidet er oppløsningspotensialet og levetiden til oksider av rutenium og tantal undersøkt. For å kartlegge hvilken effekt tantal og partikkelstørrelse har på stabiliteten, ble det brukt små mengder tantal, og katalysatorene ble lagt på en bærer av antimondopet tinnoksid, ATO. Dette gir en svært liten partikkelstørrelse, og gjør det mulig å undersøke små mengder av katalysator som frigjør lite ny overflate under degradering.

Katalysatorne ble syntetisert med en normal polyol metode. $RuCl_3$ og $TaCl_5$ ble redusert i etyleneglykol, EG, før metallpartiklene ble deponert på ATO. Katalysatorene ble undersøkt med syklisk og lineær voltammetri. Videre ble levetiden til fire katalysatorer kartlagt med kronoamperometri ved 1.455V vs. RHE. Sammensetning og mengden katalysator på bæreren ble bestemt med energidispersiv røntgendiffraksjon (EDS) og partikkelstørrelsen ble funnet med transmisjons elektronmikroskopi (TEM).

I en av syntesene ble reduksjonstiden og -temperaturen økt fra 3 timer ved 170°C til 4 timer ved 190°C for å øke reduksjonshastigheten. Dette hadde ingen effekt på Ta konsentrasjonen, men resulterte i en fraksjon av amorf fase som ikke ble observert i noen av de andre katalysatorene. De amorfe $Ru_{0.9}Ta_{0.1}O_2$ partiklene hadde den største partikkelstørrelsen og den beste stabiliteten av de undersøkte. 10wt% vann ble tilsatt syntesen av en ATO-RuO_2 katalysator for å øke partikkelstørrelsen, men ingen signifikant effekt ble observert. RuO_2 med en større partikkelstørrelse og de amorfe $Ru_{0.9}Ta_{0.1}O_2$ partiklene ble syntetisert ved a sedimentere ut partikler uten bærer.

Tilsetningen av tantal har en negativ effekt på katalytisk aktivitet. Når Ta er til stede, får oppløsningspotensialet til Ru rundt 1.45V en svak økning, men degraderingshastigheten øker på potensial over 1.49V. En større partikkelstørrelse i RuO_2 har en signifikant positiv effekt på stabilitet.

Abstract

The most active catalyst for oxygen evolution in PEM water electrolysis is ruthenium oxide. Its major drawback as a commercial catalyst is its poor stability. In a mixed oxide with iridium, ruthenium becomes more stable. However, it would be favorable to find a less expensive substitute to iridium. In this work, the dissolution potential and lifetime of mixed oxides containing ruthenium and tantalum are investigated. In order to effectively determine what effects tantalum and particle size have on stability, only a small amount of tantalum is used, and the catalysts are supported by antimony doped tin oxide, ATO. This leads to a very small particle size, and makes it possible to investigate small amounts of catalyst where little new surface is made available during degradation.

Catalysts were prepared with the normal polyol method by reducing $RuCl_3$ and $TaCl_5$ in ethylene glycol, EG, before the metal particles were deposited on the ATO support. The catalysts were investigated electrochemically with cyclic and linear voltammetry. Furthermore, the lifetime of four catalysts were determined by chronoamperometry at 1.455V vs. RHE. The compositions and loading of catalyst on the support were determined by energy dispersive x-ray spectroscopy (EDS) and the particle sizes were measured with transmission electron microscopy (TEM).

In one synthesis, the reduction time and temperature were increased from 3 hours at 170°C to 4 hours at 190°C in order to increase the reduction rate. While this had no effect on the Ta composition, the catalyst got a fraction of amorphous phase not found in any of the other catalysts. The amorphous $Ru_{0.9}Ta_{0.1}O_2$ particles had the largest particle size and the highest stability of the ones investigated. 10wt% water was added to the synthesis of an ATO-RuO_2 catalyst in order to increase the particle size, but no significant effect was observed. Larger RuO_2 particles and amorphous $Ru_{0.9}Ta_{0.1}O_2$ particles were obtained by collecting them as unsupported catalysts.

The addition of tantalum has a negative effect on the catalytic activity. When Ta is present, the dissolution potential of Ru at around 1.45V is slightly increased, but the degradation rate is increased above 1.49V. A large particle size in RuO_2 has a significant positive effect on stability.

Contents

1 Introduction

It has long been predicted that hydrogen will play an important role as a clean and efficient energy carrier as the price of fossil fuels increases due to increasing demand and decreasing reserves. In order to realize this prediction, a convenient type of electrolyzer and fuel cell will have to be commercialized. A water electrolysis cell will split water into hydrogen and oxygen gas when electricity is applied, thus transforming electricity into a portable, efficient fuel. A fuel cell is doing the opposite by recombining hydrogen and oxygen with energy and water as the product. When combined with clean, renewable energy sources a sustainable energy system can be implemented, free from carbon emissions [1]. An illustration is given in Figure 1.1.

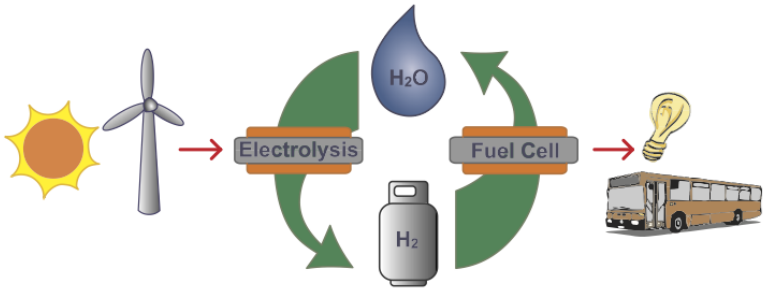

Figure 1.1: Illustration of a sustainable energy system based on renewable energy sources [1].

Water electrolysis with a proton exchanging membrane (PEM) provides hydrogen gas safely and efficiently with a high purity [2]. So far the cost of this process has prevented the technology from reaching out to the regular consumer. In order to reduce these costs it is favorable to use a smaller amount of catalyst without compromising the overall activity or the lifetime of the catalyst layer. In this work catalysts for the oxygen evolution reaction will be studied. This reaction is the rate limiting factor in water electrolysis, and is the main reason for the required overpotential in the process [3].

The catalysts used for the oxygen evolution reaction are made of noble metal oxides. These metals are expensive, so in order to increase the cost efficiency it would be desirable to have catalysts with a large surface area per unit of mass. To prevent the metal nano particles from agglomerating during the synthesis, it is possible to support it with a larger set of conductive particles [4]. Previous work at NTNU has shown that antimony doped tin oxide, abbreviated ATO, can fill the role of an effective support for oxygen evolution catalysts.

Ruthenium oxide is the most active known catalyst for the oxygen evolution reaction. Unfortunately, $RuO2$ is highly unstable at higher potentials, and the activity is lost due to dissolution of the catalyst [5, 6, 7]. Iridium has been proved to have a stabilizing effect on ruthenium [8], but due to the high price, it would be beneficial to find another element with the same stabilizing properties. Tantalum has been suggested as an alternative [9], but due to the lack of a standardized and effective method of measuring the stability of an oxygen evolution catalyst, it has still not been shown that this is the case.

Degradation mechanisms in oxygen evolution catalysts are still not widely understood, and multiple mechanisms are active simultaneously. In this work the focus will be on degradation by dissolution of ruthenium, and how this is defined by the particle size and the Ta-composition. In order to produce comparable samples with differences in the mentioned properties, three variations of the reduction step in the normal polyol synthesis route were applied and will be investigated in this report.

2 Theory

2.1 PEM water electrolysis

By splitting water in an electrolytic cell, hydrogen and oxygen gas is developed at the cathode and the anode respectively. When a DC voltage is applied to the electrolyzer, O_2, H^+ and electrons are produced at the anode. The electrons flow through an external circuit and H^+ travel through a wet polymer electrolyte to the cathode, where it recombines with an electron and form hydrogen gas [10]. A schematic of a PEM electrolyzer is given in figure 2.1, and the cell reactions is given below.

$$\text{Cathode reaction} \qquad 4H^+ + 4e^- \rightarrow 2H_2 \tag{2.1}$$

$$\text{Anode reaction} \qquad O_2 + 4H^+ + 4e^- \leftarrow 2H_2O \tag{2.2}$$

$$\text{Total reaction} \qquad 2H_2O \rightarrow 2H_2 + O_2 \tag{2.3}$$

The oxygen evolution reaction (2.2) has a reversible potential with the same dependence on pH as hydrogen evolution (2.1). When the electrodes are exposed to the same electrolyte, as in a PEM electrolytic cell, the reversible potential difference will be 1,23V. However, an electrolytic cell is usually operated at a potential above the thermoneutral voltage, which is 1.482V [11]. At this voltage the electrical energy covers both the energy for the electrochemical reaction and the required thermal energy. At potentials below the thermoneutral voltage, heat is provided by the surroundings.

Because of the high operating potential on the anode, the oxygen evolution catalyst must tolerate a very corrosive environment. This means that only stable metal oxides can be used. It is important that the oxides are conductive as well, as current must be lead to the external circuit.

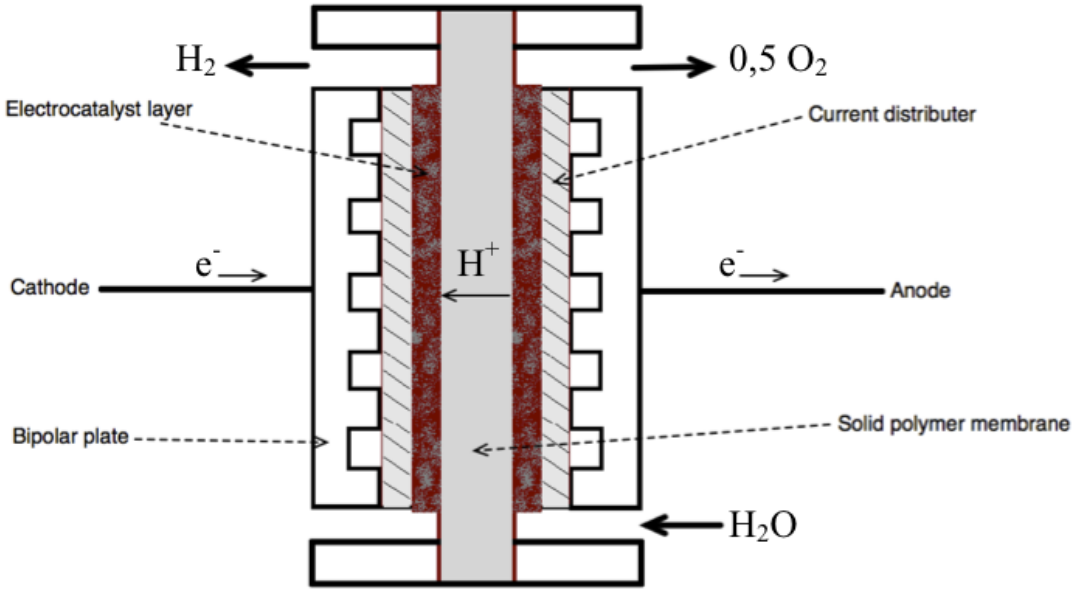

Figure 2.1: A schematic showing the principle of a PEM electrolytic cell.

2.2 Oxygen evolution

Several mechanisms for the oxygen evolution reaction have been suggested [12, 13]. All the mechanisms will not be mentioned here, but a general overview will be given and an example of a reaction path will be discussed later in section 2.4.2. The reaction can be divided into three steps: adsorption, charge transfer and desorption. The kinetics will be determined by the slowest mechanism, or what is known as the *rate determining step*. Matsumoto and Sato [13] suggested that M-O bond strength is determining the adsorption and desorption rates. A high M-O bond strength will result in fast adsorption and slow desorption. By the same argument will weak bond strengths lead to slow adsorption and fast desorption. Thus, an intermediate bond strength that favors both adsorption and desorption is desirable. The electron transfer rate is mainly determined by the density of electron states at the Fermi level and the degree of orbital overlapping of the active sites and the adsorbed species [13].

To summarize, the reaction rate of oxygen evolution is determined by the material properties of the surface species at the electrode. The volcano plot in figure 2.2 compares the catalytic activity of different oxides. Here, the electrocatalytic activ-

ity (measured as anodic overpotential) is related to the enthalpy for the oxides to form a higher oxidation state from a lower oxidation state. This could be directly related to the M-O bond strength.[5].

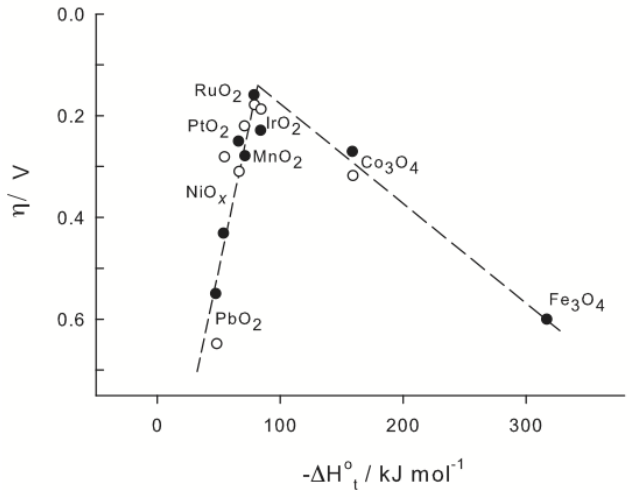

Figure 2.2: Volcano-plot of electrocalalytic activity of different oxides in acidic (open spheres) and alkaline (filled spheres) solutions [1].

The reaction will most likely happen at a surface defect, or an *active site*, so the reaction rate will also depend on the number of available sites. The number of active sites is given by the surface area of the catalyst. To get a larger area with the same amount of noble metal, the particle size should to be small.

2.3 The polyol synthesis method

The polyol synthesis method can be utilized to produce noble metal nano crystals. A polyol is an alcohol with multiple –OH groups, and is used as both a solvent and a reducing agent to a metal precursor. A commonly used polyol is ethylene glycol (EG). Bock et al. [14] successfully reduced Pt and Ru salts in EG at elevated temperatures, before depositing the colloids on a carbon support. The reduction mechanism is illustrated in Figure 2.3. The –OH groups in EG (A) interact with the metal cations and are reduced to aldehyde groups (B and C). The aldehydes are unstable and will further oxidize to glycolic (D) and oxalic acid (E). The two carboxylic acids may be further oxidized to CO, CO_2 or CO_3^{2-} in alkaline solutions. The electrons donated in these oxidation reactions result in reduction of the metal cations to metal atoms. The final result of the reduction step is then nano sized

metal particles dispersed in EG with a mixture of the reaction products mentioned above.

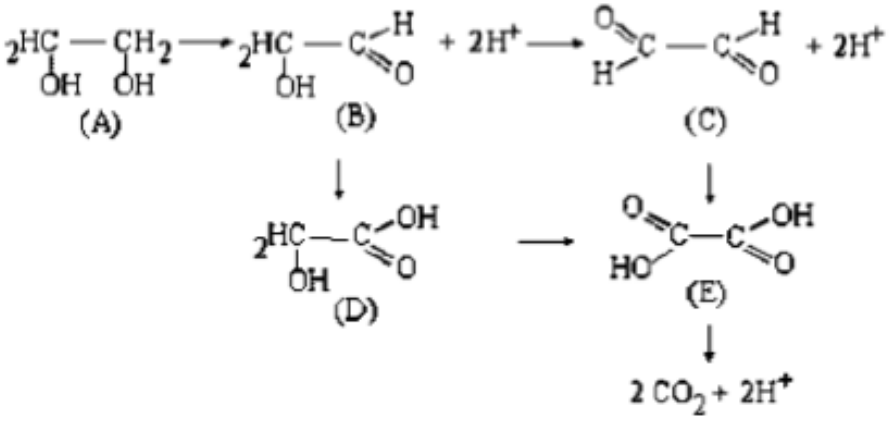

Figure 2.3: Reduction mechanism of precursor salts, accompanied by oxidation of ethylene glycol[14].

The total oxidation reaction of EG in reaction (2.4) can be used to determine the minimum temperature needed to reduce the metal cations [15]. Since ruthenium is a noble metal, ruthenium chloride has a positive reduction potential and thermodynamics dictate that EG will reduce it at room temperature. Tantalum however has a negative reduction potential, meaning that thermal energy is required to reduce it. Assuming EG is oxidized to $CO_{(g)}$, as in in equation 2.4, ΔG can be plotted as a function of temperature for different activities of HCl and $TaCl_5$. This is shown in figure 2.4 and indicates that reduction of tantalum is only possible at high temperatures. This figure is only an illustration as the calculations do not consider that the produced H^+ ions interact with OH^- ions in the alkaline solution and it does not include the buildup of Cl^--ions from the reduction of $RuCl_3$. It does, however, include realistic concentrations based on the experiments in this work. The highest possible temperature is the boiling point of EG, 197°C [15]. As Ta^{5+} is reduced the concentration of $TaCl_5$ decreases and the concentration of HCl is dramatically increased.

$$\frac{6}{5}TaCl_5 + C_2H_6O_2 = \frac{6}{5}Ta + 2CO + 6HCl \tag{2.4}$$

Grolleau et al. [16] synthesized Pt particles on a carbon support and suggested another aspect to reduction process. The reducing agent is not EG itself, but a product of a dehydration reaction that is catalyzed by OH^--ions and activated at elevated temperatures. This reaction is given in equation (2.5). The concentration

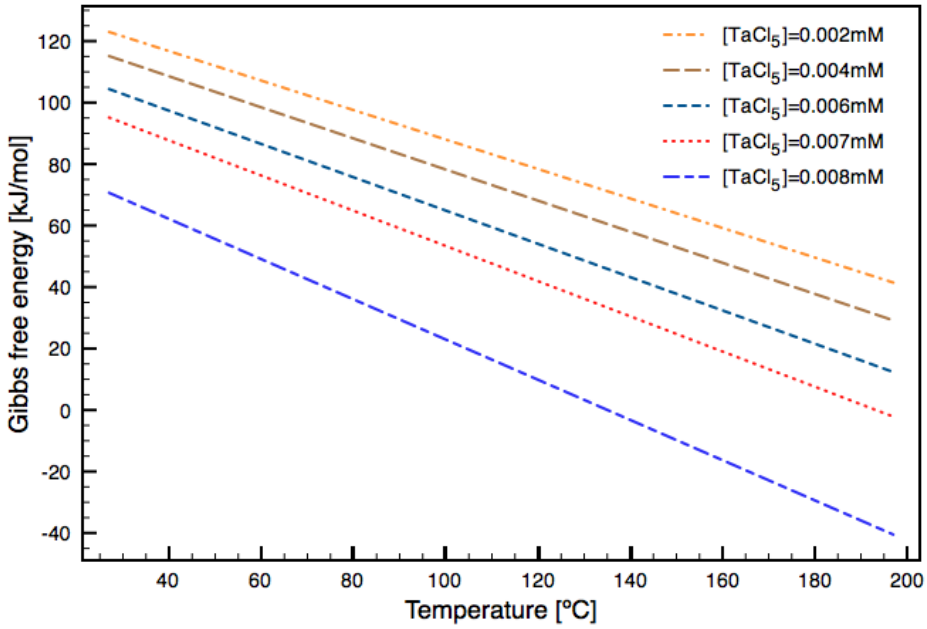

Figure 2.4: Thermodynamic equilibrium calculations from reaction (2.4). When ΔG is negative, reduction of $TaCl_5$ is possible. Realistic concentrations based on the experiments in this work are applied. The pH and the build up of $[Cl^-]$ from reduction of $RuCl_3$ are not considered.

of the reducing agent, acetaldehyde, then determine the reduction rate of the metal ions and how fast new nuclei are created. This means that a fast or a slow reduction rate will lead to small or large particle sizes respectively. By this argument, a high temperature and a high pH will result in a small particle size. Water is also produced in reaction (2.5), indicating that a low activity of water should enhance the production of acetaldehyde, thus increasing the reduction rate.

$$CH_2OH - CH_2OH \leftrightarrow CH_3 - COH + H_2O \tag{2.5}$$

When Grolleau et al. [16] tried to lower the reduction pH, it was found that less glycolate was produced in the reaction medium and that this could be explained by the chemical equilibrium given in reaction (2.6). Glycolate is a surfactant, which means it binds to the metal surface and changes the interfacial tension between the particles and the liquid reaction medium [17]. In Grolleau´s case, this had an effect on the particle morphology.

$$CH_2OH - CH_2OH + 2OH^- \leftrightarrow CH_2O^- - CH_2O^- + H_2O \tag{2.6}$$

After the reduction step the metal colloids must be extracted from the solution. By tailoring the pH, one can also change the surface charge of the particles. In aqueous solutions, this is due to adsorption of H_3O^+ and OH^- on the surface. This results in negatively charged particles in alkaline solutions and positively charged particles in acidic. The pH where the charge is zero is called the *Point of Zero Charge* (PZC) [10]. At PZC there is no electrostatic forces between equal particles, and they will agglomerate. In the case where the product contains only one element, this is the optimal pH. In this work however, the metal particles should be small and well dispersed on the surface of the support. The optimal pH would then be between the PZC for the support and the metal particles. This means that the particles and the support is charged oppositely, and the attractive forces will ensure an even dispersion of particles on the support surface.

When extracting the catalyst particles from EG, the mechanisms are more complicated. When lowering the pH, the water content in the EG also changes, which in turn changes the PZC of the particles. In addition to the electrostatic forces, there are other effects that may arise in the presence of a surfactant. Since the reduction step takes place at a high pH, glycolate will be present. The surfactant adsorbs on the particle surface and gives rise to osmotic pressures and physical forces between the particles [17]. As a consequence, the particles repel each other and deposition becomes difficult. By lowering the pH, glycolate can be combined with H^+ forming glycolic acid or react back to EG. The surfactant is then removed, and deposition becomes easier.

2.4 Electrochemical characterization

2.4.1 Cyclic voltammetry

Cyclic voltammetry involves changing the potential at the working electrode at a constant sweep rate, ν, between an upper and a lower limit while measuring the current [18, 10]. The schematic in figure 2.5 shows the potential-time behavior on the working electrode. In aqueous electrolytes the turn-round potentials are usually chosen to lie between the hydrogen and oxygen evolution potential. In this way impurities can be removed by oxidation or reduction and no gas bubbles are evolved; in both cases preventing blocking of the electrode surface [10].

In the current-potential plot, *the cyclic voltammogram*, peaks can be observed that correspond to the formation or dissolution of chemisorbed hydride and oxide layers

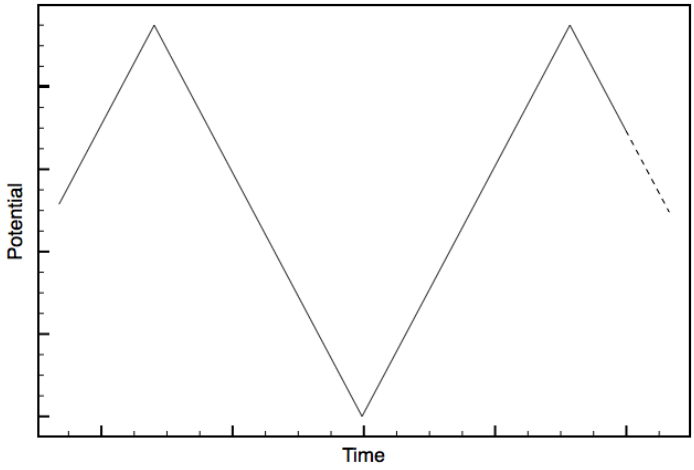

Figure 2.5: Potential-time behavior at the working electrode during cyclic voltammetry. The slope, ν, is the sweep rate in [mV/s].

on the electrode surface. Although the shape of the cyclic voltammograms depends on parameters like electrolyte purity, turn-round potentials and sweep rate, they are highly reproducible.

In the cyclic voltammograms, current peaks with height I_p can be observed. The peaks correspond to an adsorption and desorption of oxygen ions and protons, leading to an oxidation or a reduction of the metal cations on the electrode surface. The peak current, I_p gets higher with increasing sweep rate. If the electron transfer step is fast, the peak potential, E_p, is independent of sweep rate. On the contrary, if the electron transfer is slow E_p will increase with increasing sweep rate, simply because the electrochemical reaction cannot keep up with the potential change [10]. The effect of an increased sweep rate is shown in figure 2.6.

The voltammograms in figure 2.6 are recorded in this work, and show a typical behavior for ruthenium oxide [19, 20, 21]. The oxidation/reduction processes corresponding to the two peaks in figure 2.6 are related to the oxidation of Ru to $Ru(OH)_3$, and RuO_2 [7]. Tantalum, which will also be used in this work, easily forms Ta_2O_5. Because of low Ta-compositions, tantalum atoms are assumed to substitute ruthenium atoms in the rutile crystal lattice of RuO_2 forming $Ru_{1-x}Ta_xO_2$.

From Fick´s 2nd law of diffusion, the peak current, I_p, is proportional to the square root of sweep rate, $\sqrt{\nu}$, in the case where the electrochemical reaction is diffusion controlled [18]. Fick´s 2nd law assumes planar diffusion, not spherical, but the

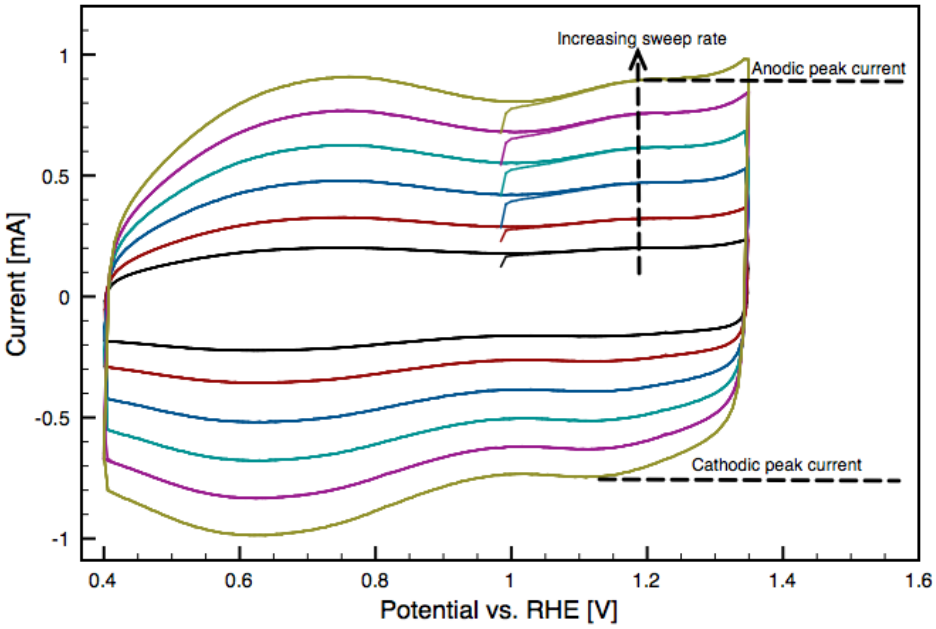

Figure 2.6: Cyclic voltammograms of ATO-supported ruthenium oxide. Increased sweep rate gives an increased peak current. The potential where the current peak is located is known as the peak potential.

difference is assumed to be negligible for the catalysts investigated in this work. If, however, the oxidation/reduction is determined by adsorption processes rather than diffusion, the peak current is proportional to ν, and not $\sqrt{\nu}$. The actual values of I_p, E_p and the peak width are in this case dependent on the type of adsorption isotherm involved and the adsorption strengths of the active species [18].

Information about the reversibility of the adsorption/desorption processes can be found from the anodic and cathodic peak potentials. When the adsorption is reversible the anodic and cathodic peaks are symmetrical and happen at the same potential. The other extreme is the irreversible case, where the anodic peak is non- symmetrical and the cathodic peak is absent, indicating no desorption at all. In most cases the adsorption is quasi-reversible where both peaks are present, but not symmetrical, and there is a small difference in the peak potentials [10].

The reversibility can also be investigated from the net charge in the voltammograms. For completely reversible adsorption the charge and discharge is of the same value, giving no net charge.

2.4.2 Linear sweep voltammetry

Polarization curves are obtained by linear sweep voltammetry, which involves changing the potential with a constant sweep rate while measuring the current response. These curves reflect the steady state conditions, hence a low sweep rate should be used. When obtaining a polarization curve for the oxygen evolution reaction, the potential is swept in the potential region where oxygen is evolved, above 1.23V. At high potentials the surface concentration of the active species is zero, and the current is controlled by diffusion from the electrolyte to the surface. At this point the current will reach a *limiting current*. Further increase of the potential will only lead to charging of the electrode. To increase the limiting current it is possible to apply rotation to the electrode, which will give a smaller diffusion layer thickness [10].

From the polarization curves, Tafel slopes and exchange current densities can be determined. A good catalyst has a high exchange current density and a low Tafel slope. These criterions give a low overpotential for a given current density. The Tafel equation is given below [10].

$$\eta = a + blog|i| = blog\frac{|i|}{|i_0|} \tag{2.7}$$

Here, η is the overpotential, b is the Tafel slope and i is the current density. The exchange current density, i_0, is the current density at zero overpotential, $E = E^{rev}$. This is found by extrapolating the linear Tafel curve to the reversible potential. i_0 can not be measured directly because the anodic (positive) and cathodic (negative) exchange currents are oppositely equal at the reversible potential, giving no net current.

The Tafel slope can provide useful information about the rate determining mechanism in the system [12, 13]. Three reactions are listed below, and together they describe the total reaction of oxygen evolution. The Tafel slope for each mechanism can be calculated by assuming the respective reaction is rate determining. In that way, the calculated Tafel slopes can be compared to experimental data to find the rate determining step in the experiment. The respective Tafel slopes are listed together with the reaction mechanisms below [22].

$$S + H_2O \rightarrow S - OH_{ads} + H^+ + e^- \qquad b = 120mV/dec \tag{2.8}$$
$$S - OH_{ads} \rightarrow S - O_{ads} + H^+ + e^- \qquad b = 40mV/dec \tag{2.9}$$
$$S - O_{ads} \rightarrow S + \frac{1}{2}O_2 \qquad b = 30mV/dec \tag{2.10}$$

S represent an active site on the oxide surface. OH_{ads} and O_{ads} represent two adsorbed species on the surface.

2.5 Normalization of current

When comparing catalysts, it is necessary to isolate the catalytic activity from variables like the electrode loading and the surface area of the catalyst particles. Two common methods are to normalize the current with respect to the electrochemically active surface area (EASA) and the mass of metal catalyst applied to the electrode. The first method will give a scientific measure of the properties of the catalyst materials. The latter can be seen as the more practical of the two, as it reflects the differences in the synthesis route combined with the catalyst composition.

2.5.1 EASA - Specific catalytic activity

From the cyclic voltammograms at different sweep rates, the adsorption charges can be found by integrating the current with respect to time. These charges are expected to decrease with increasing sweep rates as seen in figure 2.7. At low sweep rates, the protons have time to diffuse into pores, cracks and grain boundaries in the oxide, thus increasing the amount of material available for oxidation or reduction. At higher sweep rates the diffusion time is decreased and only the more accessible active sites close to the surface remains available [23]. As long as the kinetics is determined by diffusion into these pores and cracks, this can provide a quantitative measure of the active surface area.

The charge, q, is a function of the diffusion time and has been shown to be inversely proportional to $\sqrt{\nu}$. A linear relationship occurs when $1/q$ is plotted against $\sqrt{\nu}$ and q is plotted against $1/\sqrt{\nu}$. If the lines are extrapolated to the y-axis, the charge at zero and infinite sweep rate can be found. This can be seen as the total and outer charge respectively, where the outer charge is directly connected to the active surface area of the catalyst. The inner charge can be found from the difference between the outer and the total charge.

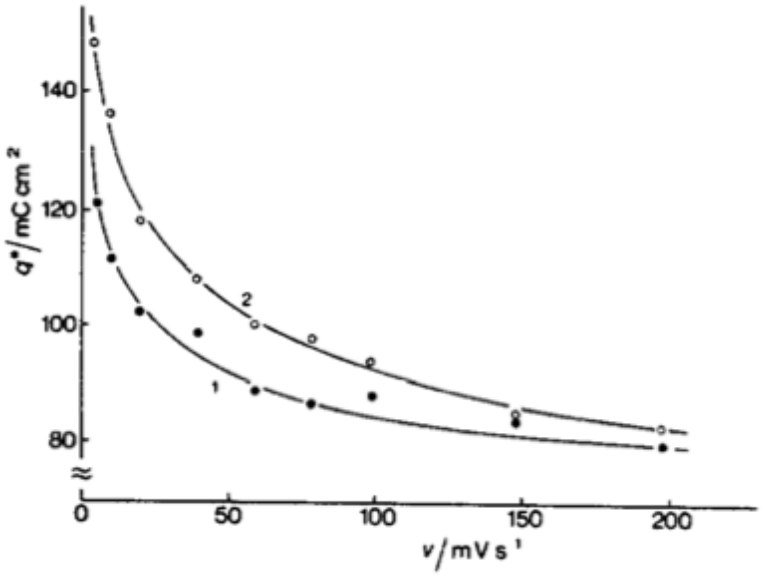

Figure 2.7: Sweep rate dependence on charge in CVs, given that diffusion is important [23].

If diffusion is not a rate determining factor, the assumption that this method is based on is invalid. Without diffusion control the active surface area, and thus the charge, should be independent of sweep rate. In this case the charge at the highest sweep rate, 300mV/sec, is used as a normalization factor and will be referred to as q_{300}.

2.5.2 Mass of metal catalyst - Catalytic activity

By normalizing the current with respect to the mass of metal catalyst, the *catalytic activity*, can be found. This provides a simple, but effective, normalization method seen with commercial interests, as the catalyst mass reflects the cost of the anode. In this work 20μl of a 2mg/ml solution was added to the electrode. With the assumption that the catalyst dispersion is completely homogenous, 40μg of catalyst was applied to the electrode. The catalytic activity can then be expressed with equation (2.11). The metal loading on ATO is given in weight fraction and expressed with $x_{catalyst}$. To get a comparable value of the catalytic activity, a suitable potential is chosen and the current at this potential is divided by the applied mass.

$$\text{Catalytic activity}[mAmg^{-1}] = \frac{I}{0.004mg \times x_{catalyst}} \tag{2.11}$$

2.6 Catalyst stability

There are many factors that contribute to degradation of a catalyst layer. Wu et al. [24] summarizes the following degradation mechanisms for Pt-based catalysts in PEM fuel cells:

- Dealloying of electrocatalyst
- Corrosion of electrocatalyst support
- Mechanical stress
- Contamination
- Change in hydrophobicity due to Nafion dissolution

Platinum is also commonly used for hydrogen evolution in electrolysis, but for the oxygen evolution catalysts only oxides are stable at the high potentials. A similar set of mechanisms would apply for the oxides. Contamination can be a problem in fuel cells and on hydrogen evolution catalysts because the contaminations cannot be removed with oxidation. Most contaminations on the oxygen evolution catalyst, however, will be removed due to the high potential. When the produced gas bubbles are removed from the electrode surface, the catalysts are exposed to a mechanical stress that can lead to degradation. Corrosion of the catalyst support is an important factor in oxygen evolution. Since carbon oxidizes easily, it is necessary to use a more stable support. This is one of the reasons why ATO is used in this work. The most important mechanism in this work is dealloying of the electrocatalyst, or more specifically dissolution of ruthenium.

The pourbaix diagram [7] for ruthenium is given in figure 2.8. It shows the electrochemical equilibria in the system as the function of pH and potential. In an acidic environment, Ru is oxidized with the electrochemical and chemical equilibrium reactions listed below. The product of reaction (2.15), H_2RuO_5, is soluble in water and is responsible for the dealloying of the catalyst.

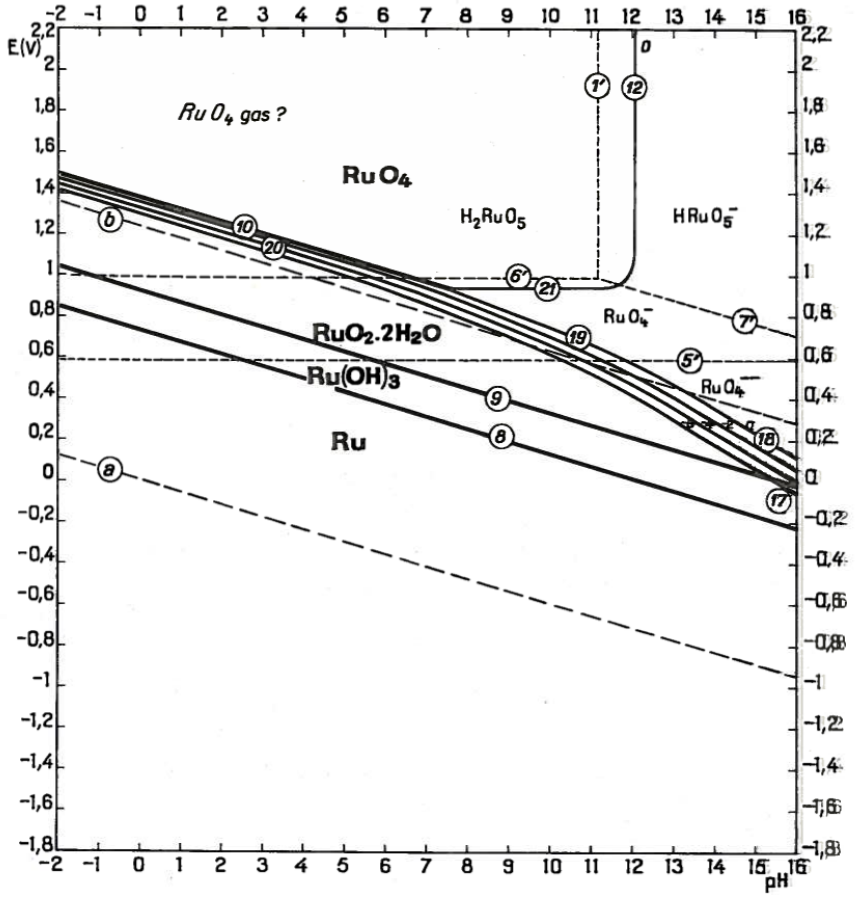

Figure 2.8: Pourbaix diagram for ruthenium. Ru_2O_3 and RuO_2 are written in their hydrated form. Oxygen evolution is possible at potentials above the line labeled *b*. [7]

$$2Ru + 3H_2O = Ru_2O_3 + 6H^+ + 6e^- \qquad E^{rev} = 0.738 - 0.0591pH \qquad (2.12)$$

$$Ru_2O_3 + H_2O = 2RuO_2 + 2H^+ + 2e^- \qquad E^{rev} = 0.937 - 0.0591pH \qquad (2.13)$$

$$RuO_2 + 2H_2O = RuO4 + 4H^+ + 4e^- \qquad E^{rev} = 1.387 - 0.0591pH \qquad (2.14)$$

$$RuO_4 + H_2O = H_2RuO_5 \qquad log(H_2RuO_5) = -0.88 \qquad (2.15)$$

Dissolution of ruthenium is possible at potentials above 1.387V vs RHE. This is much lower than the desired operating potential during electrolysis. When ruthenium is alloyed with iridium, the most corrosive sites in the rutile crystal lattice get occupied by iridium, which is stable at higher potentials [8]. This prevents the dissolution of ruthenium, thus stabilizing the catalyst. The polarization curves in

figure 2.9 are a part of a previous study of ATO supported $Ir_{1-x}Ru_xO_2$ catalysts. In these curves the current drops at a given potential because the ruthenium is rapidly dissolved. This given potential is increased when 20at% iridium is added to the catalyst, illustrating the stabilizing effect of iridium. The potential corresponding to the current peak can be seen as measure of how fast ruthenium is dissolving because the current drop is a direct consequence of the removal of active mass. This potential will be seen as the dissolution potential of ruthenium and will be used in the investigation of stability with respect to tantalum and particle size.

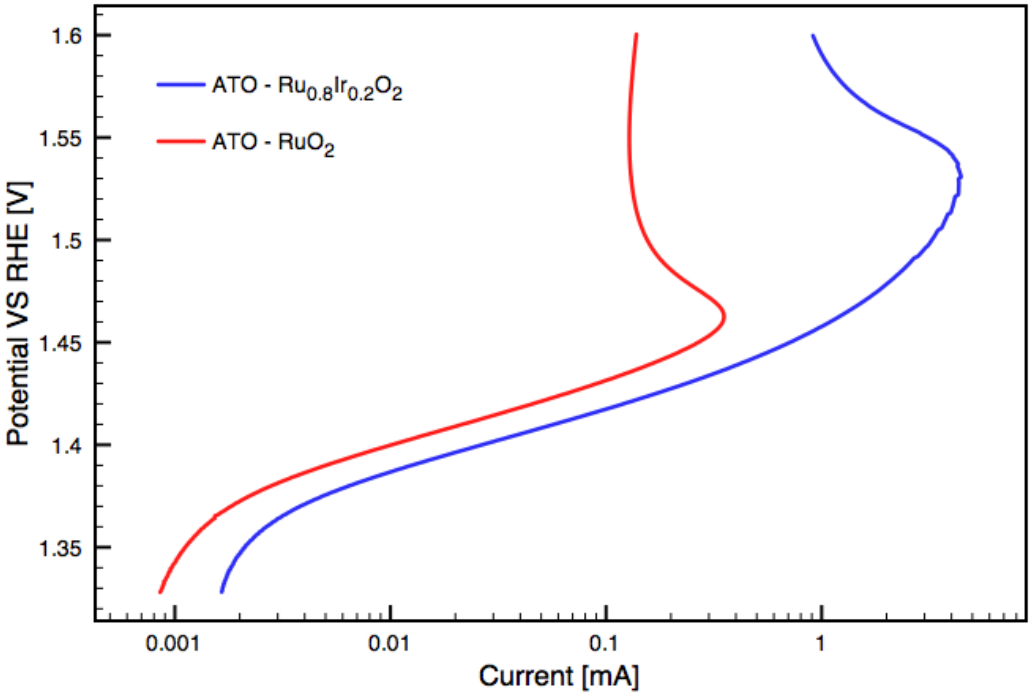

Figure 2.9: Polarization curves of ATO-supported RuO_2 and $Ru_{0.8}Ir_{0.2}O_2$. The peak current happens at a higher dissolution potential when iridium is added to the catalyst.

3 Experimental

3.1 Synthesis

Table 3.1: Equipment and chemicals used in synthesis.

Chemicals	Equipment
-Ethylene glycol, Sigma Aldrich	-Three necked round bottom flask
-$NaOH$, Merck	-Hotplate and magnetic stirrer for round bottom flask, IKA
-$TaCl_5$, anhydrous 99.99%, Alfa Aesar	-Condenser
-$RuCl3$, anhydrous 99%, Alfa Aesar	-Oven, Termaks
-ATO, <50nm, >99.5%, Zigma Aldrich	- Centrifuge, Biofuge primo, Heraeus Instruments
-N_2, AGA	-pH meter, pH/Ion meter, Methrom
	-Digital Sonifier, Brandson

The synthesis route used in this work is called a normal polyol method and a schematic is shown in figure 3.1. The synthesis is divided into two steps: reduction (1-5) and deposition (6-9). Before start, the glassware was dried together with ATO and NaOH at 120°C over night. 200mg of dry NaOH was dissolved in EG in the reaction vessel (1) and the precursor salts are weighed out and added to the reaction vessel (2). The total volume of EG was 50ml. The EG is stirred at 250rpm, bubbled with nitrogen and heated under reflux during the whole synthesis. Precautions were made to control the water content in the system. In order to reduce the metal precursors, the solution was heated to 170°C for 3 hours (3). In one of the experiments an additional 6ml of deionized water (10wt%) were added before NaOH were dissolved (1). In another, the solution was heated to 190°C for 4 hours (3). These two changes to the synthesis were meant to increase the particle size and the tantalum composition, respectively.

Dry ATO was dispersed in 30 ml EG with a digital sonifier at 20% amplitude for 8 minutes (4) and mixed into the reaction vessel during sonication at 80°C (6). The pH was lowered to around 0.4 with sulfuric acid in all the experiments with the exception of the synthesis with 10wt% water. In this synthesis the pH was lowered to 0.95 because a large buffer capacity was observed starting at pH1.5. The temperature was kept over night at 80°C under reflux with N_2 bubbling and stirring at 250 rpm (7). The solution was then separated in a centrifuge, followed by washing of the product several times in hot water (8). Finally, it was dried over night at 120°C (9). The aim was a loading of 20wt% catalyst on the support.

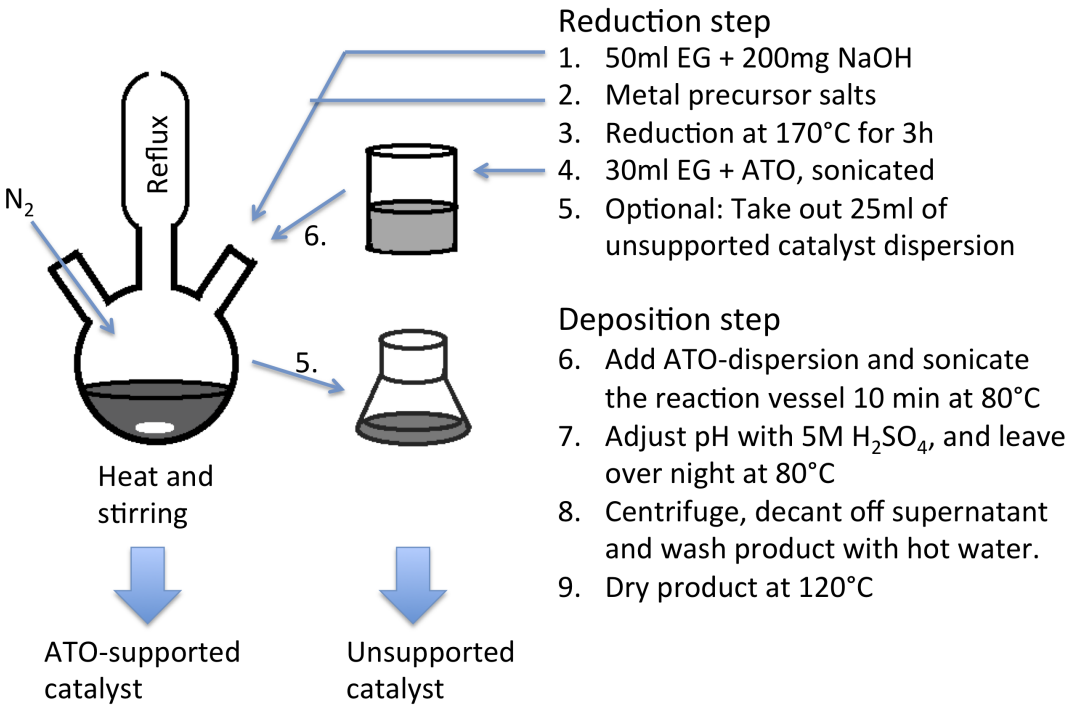

Figure 3.1: A schematic showing the polyol synthesis route in steps.

After the reduction step, 25ml of the EG was taken out of the reaction vessel in two of the experiments (5): one RuO_2 catalyst and one nominal $Ru_{0.6}Ta_{0.4}O_2$ catalyst. In these experiments the pH was lowered with 5M H_2SO_4 to around 0.5, the dispersions centrifuged and the product washed with hot water and dried at 120°C. The RuO_2 catalyst was given a long time to agglomerate in order to get more catalyst out of the EG. This resulted in two unsupported catalysts which had been through the same reduction steps as their supported versions. The two unsupported catalysts came from the two experiments mentioned earlier. One RuO_2 catalyst made with 10wt% water in the synthesis, and a $Ru_{1-x}Ta_xO_2$ catalyst was synthesized by reduction at 190°C for 4 hours.

3.2 Electrochemical measurements

3.2.1 Electrode preperation

The supported catalysts were dispersed with a ratio of 2mg per ml of diluted H_2SO_4 with a pH of 3. The two unsupported catalysts were dispersed with a ratio of 1mg per 4ml of water in order to get about the same loading of catalyst metal on the electrode as the supported catalysts. The dispersions were then sonicated for 45 minutes, left for at least one day and sonicated again for 5 minutes before use. A drop of 20μl was placed on a gold rotating disc electrode and the dispersant was dried off in argon atmosphere. 20μl 0.05% Nafion solution with pH3 was placed on the catalyst film and the solvent was dried off in the same manner.

Before each experiment, the cell was cleaned with deionized water and 0.5M sulfuric acid and a reference electrode was prepared. The cell was filled with 0.5M sulfuric acid and bubbled with argon gas for 30 minutes.

Table 3.2: Equipment and chemicals used in electrochemical analysis.

Chemicals	Equipment
-Sulfuric acid, 96%, Merck	-Ultrasonic bath, VWR
-Nafion, 5wt%, Alpha Aesar	-Potentiostat, VMP3 Multi Potentiostat, Biologic Instruments
-Ar(g), AGA	-RHE reference electrode
	-Pt counter electrode
	-Au rotating disc electrode, Pine Research Instruments
	-Rotating electrode speed control, Pine Research Instruments

3.2.2 Cyclic voltammetry

The CV characterization were performed in 0,5M H_2SO_4 electrolyte with a reversible hydrogen electrode (RHE) as reference. The potentiostat used were a VMP3 Multi Potentiostat from Biologic Instruments and data were recorded with EC-LAB v.10.10. The potential was swept between 0.4V and 1.35V vs RHE. The sweep rates and number of cycles follow the protocol given in table 3.3. The first sequence is designed to electrochemically oxidize the metal particles to form the metal oxide. As mentioned in section 2.4.1The tantalum ions are assumed to substitute the ruthenium ions in the rutile lattice, resulting in $Ru_{1-x}Ta_xO_2$ particles.

Table 3.3: Cyclic voltammetry protocol; number of cycles and sweep rates.

Seq. no	Sweep rate [mV/s]	# cycles	Seq. no	Sweep rate [mV/s]	# cycles
1	20	19	8	60	4
2	2	1	9	80	4
3	5	2	10	100	4
4	10	4	11	150	4
5	20	4	12	200	4
6	30	4	13	250	4
7	40	4	14	300	4

3.2.3 Linear sweep voltammetry

The linear sweep measurements followed directly after the cyclic voltammetry measurements in the same electrolyte. To remove evolved oxygen at the working electrode a rotation speed of 1200rpm was applied. The potential was swept from 1.3V to 1.6V with a rate of 0.083mV/s. After the linear sweep voltammetry, a new set of CVs were recorded by a similar protocol as the first.

3.2.4 Chronoamperometry

Since stability should be related to time in addition to a potential, supported and unsupported RuO_2 and $Ru_{1-x}Ta_xO_2$ were investigated by a chronoamperometric study. This involved keeping the potential constant, while measuring the current as a function of time. The loss of current can be related to the sum of all possible degradation mechanisms as a function of time, at a given potential. While rotating the electrode at 2000rpm, the potential was kept constant at 1.455V for 1-3 hours, depending on how quickly the current dropped.

3.3 Electron microscopy and EDS

The loading on the ATO particles and the metal concentrations were determined by a EDS-system (Energy-Dispersive X-ray Spectroscopy) from Oxford Instruments, using a Hitachi S-3400N SEM. The mass fraction of each element was calculated with Aztec from Oxford Instruments from 10 EDS spectra on each catalyst. This method provides only an approximate estimate, especially regarding the concentrations of ruthenium and tantalum due to the low relative contents compared to tin. The loading was calculated as the weight percentage of Ru and Ta metal compared to the of antimony oxide and tin oxide. The tantalum composition is given as the molar fraction of tantalum in $Ru_{1-x}Ta_x$ metal.

Pictures of the catalysts were taken in a JEM-2010 transmission electron microscope (TEM) in order to determine the size of the particles. The diameter of 100-200 particles in each catalyst were measured in the pictures. EDS was used to confirm that the particles were the ones intended, and not contaminations.

4 Results

4.1 Overview

There are three variations to the synthesis route: one reference, one with 10wt% water and one with longer time at higher temperature. Because of this, all the catalysts cannot be compared directly. The results will therefore be compared in a way that isolates one parameter at a time. Figure 4.1 illustrates the different experiments and how they will be compared to each other. The arrows in the figure represents how the catalysts are being compared.

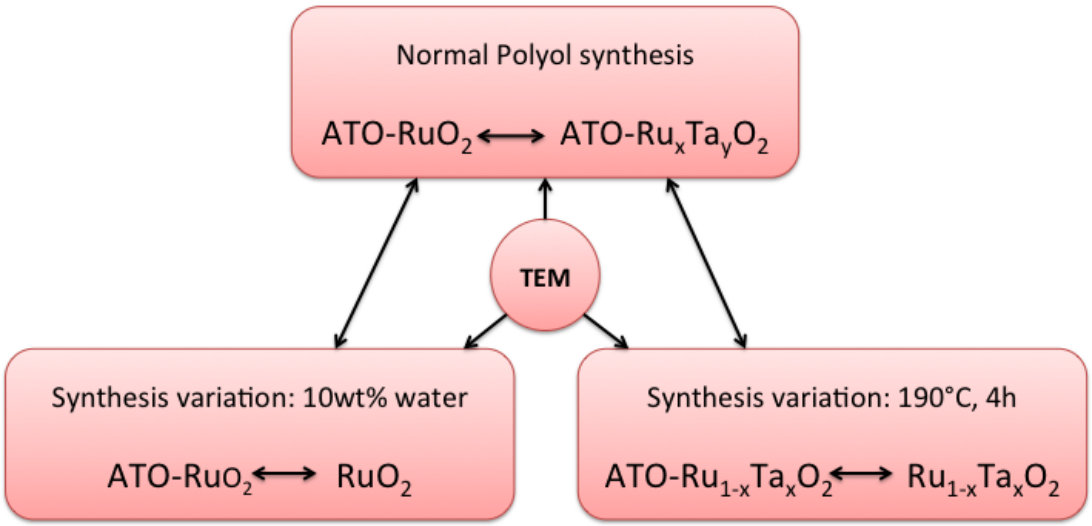

Figure 4.1: A schematic showing how the results are sorted. A box represent a synthesis variation and the arrows represent the comparisons. The circle labeled "TEM" refer to pictures taken in a transmission electron microscope.

The reference synthesis route has three ATO-supported catalysts with different tantalum compositions. The focus of this comparison is to reveal the effect of tantalum in these catalysts. The supported catalysts from the two other synthesis variations is then compared to the most similar reference catalyst to determine the effect of the synthesis parameters. Furthermore, the supported catalysts in the two variations will be compared to their unsupported counterpart in order to see the effect of the particle size and possibly the catalyst support. The pictures

taken in the TEM will provide information about the particle sizes in the different synthesis variations.

In table 4.1, the catalysts are listed along with the most important synthesis results. A lot of the $Ru_{0.6}Ta_{0.4}O_2$ catalyst was lost during weighing and it resulted in a total of 2.4mg of usable catalyst. To prevent loosing more RuO_2 than necessary, the weight and yield of C180uns: RuO_2 were not measured. The tantalum compositions and catalyst loading are determined with EDS in a SEM. The Ta composition is given as the molar percentage of the catalyst metal and the loading is given as the weight percentage of metal catalyst. This is because the oxygen composition changes with the oxidation state of ruthenium and tantalum. The data collected with EDS is given in appendix A.

Table 4.1: Synthesis characterizations.

Nominal compositions	Synthesis label	Yield	Ta comp.	Loading
$ATO - Ru_{0.8}Ta_{0.2}O_2$	C176	82%	4.4at%	20wt%
$ATO - Ru_{0.6}Ta_{0.4}O_2$	C177	74%	24at%	9wt%
$ATO - RuO_2$	C178	83%	-	12wt%
$ATO - Ru_{0.6}Ta_{0.4}O_2$	C179sup	80%	17at%	12wt%
$Ru_{0.6}Ta_{0.4}O_2$	C179uns	$\sim 5\%$	10at%	-
$ATO - RuO_2$	C180sup	83%	-	14wt%
RuO_2	C180uns	n/a	-	-

4.2 The effect of tantalum

A summary of the results obtained by cyclic voltammetry of the catalysts synthesized by the unchanged synthesis route is given in figure 4.2. Figure 4.2a show a linear relation between the peak current located at E=1.15V in the cyclic voltammograms and the sweep rate. As explained in section 2.5.1, this shows that diffusion is not important. The charge at 300mV/s will therefore be seen as a measure of active volume and will be referred to as q_{300}. The shape of the voltammograms, shown in figure 4.2b, is very similar regardless of tantalum composition. There are no new peaks appearing when tantalum is added to the catalyst, and the existing peaks are located at the same potentials as before. The voltammograms are normalized with respect to q_{300}, so the size of the voltammograms are not considered in this figure. In table 4.2 the normalization factors are given. These show that the active volume per unit of applied mass is much higher in catalysts not containing tantalum, indicating that tantalum is passivating ruthenium. Unnormalized cyclic voltammograms are given in appendix B.

Table 4.2: Normalization factors; catalyst mass applied to the electrode, $m_{catalyst}$ and the positive charge in the CV at 300mV/s, q_{300}.

Synthesis lable	at% Ta	$m_{catalyst}$	q_{300}
C176	4.2at%	$8.03\mu g$	2.167mC
C177	23.4at%	$3.53\mu g$	1.263mC
C178	-	$4.95\mu g$	2.547mC

The results from the linear sweep voltammetry in figure 4.3b show that the presence of tantalum is lowering the catalytic activity (current per unit of mass) significantly, even at only 4at% Ta. This is seen from the shift in the linear region of the curves. This shift is not seen in figure 4.3a when the curves are normalized with respect to q_{300}, so this has to do with the normalization factors given in table 4.2. The Tafel slope is increased with around 1mV/dec when tantalum is present. At around 1.45V (region 1), the dissolution potential is reached and the current begins to drop. This potential is increased by around 5mV when tantalum is present in the two compositions used in this work. It is important to note that the loading on ATO in the two tantalum containing catalysts are quite different, meaning that more oxygen gas was produced on the electrode with 4at% Ta than on the electrode with 23at% Ta.

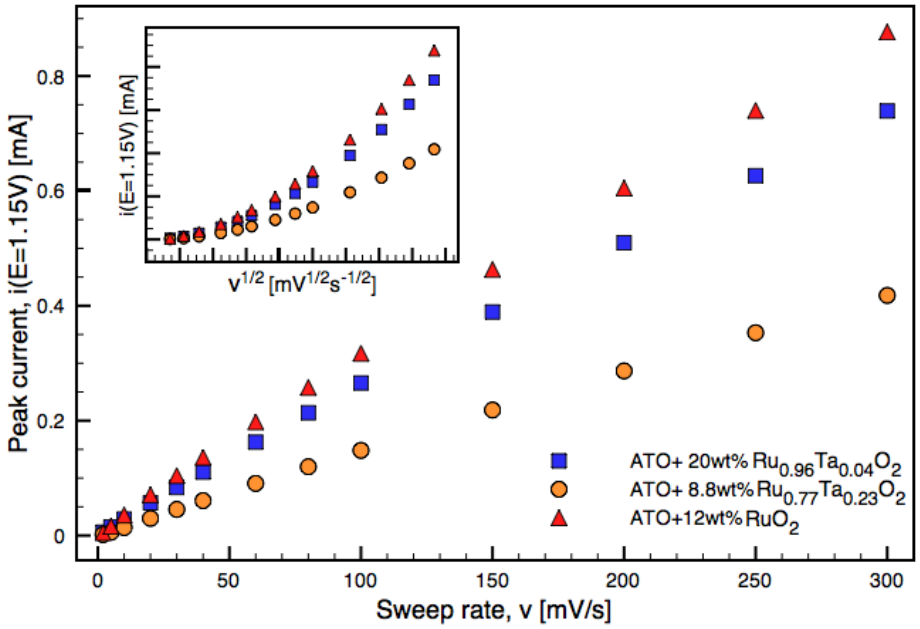

(a) Peak current, I_p, plotted against sweep rate, ν. The subplot shows I_p as a function of $\sqrt{\nu}$.

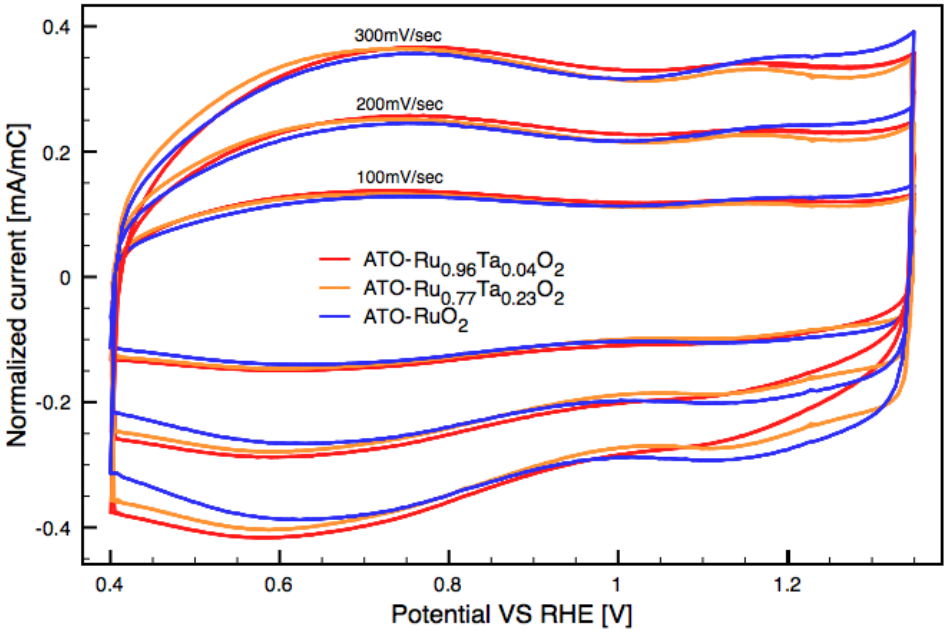

(b) Cyclic voltammograms recorded at 100, 200 and 300 mV/s. The current is normalized with respect to the charge at 300mV/s, q_{300}

Figure 4.2: Summary of data obtained by cyclic voltammetry.

Between 1.45 and 1.49V (region 2), the current from the three ATO-RuO_2 and ATO-$Ru_{1-x}Ta_xO_2$ catalysts follow a decreasing trend. ATO-$Ru_{0.96}Ta_{0.04}O_2$ decreases more quickly than ATO-$Ru_{0.77}Ta_{0.23}O_2$ in this region. This can be a consequence of the difference in loading, and therefore also the amount of produced oxygen gas on the electrode. Above 1.49V the current in the three catalysts drops more quickly and the polarization curves get a "shoulder". ATO-RuO_2 gets a much less distinct "shoulder" than the two ATO-$Ru_{1-x}Ta_xO_2$ catalysts.

A TEM-picture and the particle size distribution of C177 are given i figure 4.4. The average particle size of this catalyst is around 1.26nm, and is assumed to be representative for all the catalysts synthesized with the same synthesis route (C176, C177 and C178).

Table 4.3: Relevant values in the comparison of ATO-$Ru_{1-x}Ta_xO_2$ catalysts.

Catalyst	average E_{peak}	Tafel slope
ATO-RuO_2	1.451V	31.2mV/dec
ATO-$Ru_{0.96}Ta_{0.04}O_2$	1.456V	31.9 mV/dec
ATO-$Ru_{0.77}Ta_{0.23}O_2$	1.456V	31.6 mV/dec

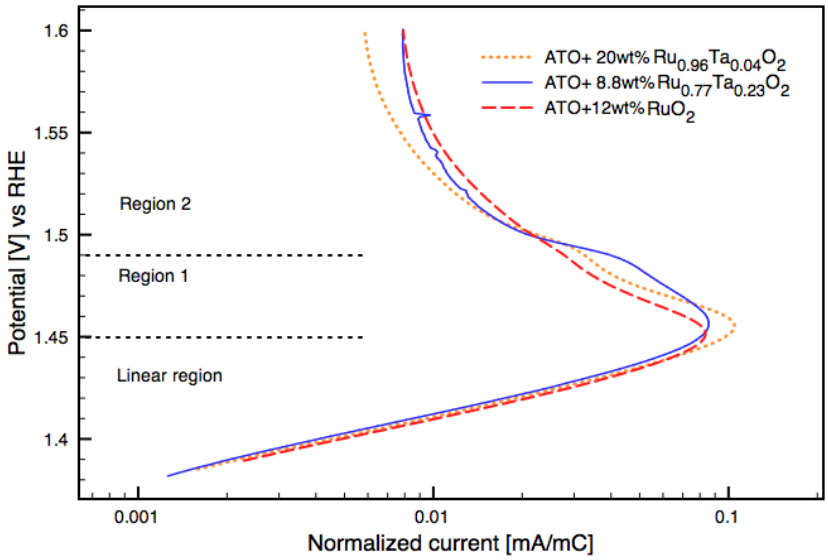

(a) Polarization curves normalized with respect to the positive charge in the corresponding CVs at 300mV/s. The curves are divided into a linear region, region 1 (1.45V-1.49V) and region 2 (>1.49V).

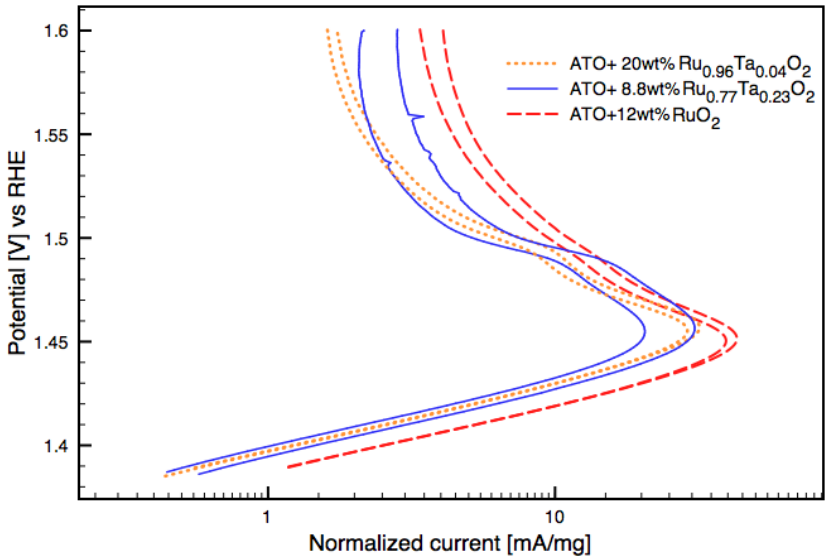

(b) Polarization curves normalized with respect to the catalyst mass applied to the electrode. Two parallels from each catalyst show the reproducibility of the experiments.

Figure 4.3: Linear sweep voltammetry

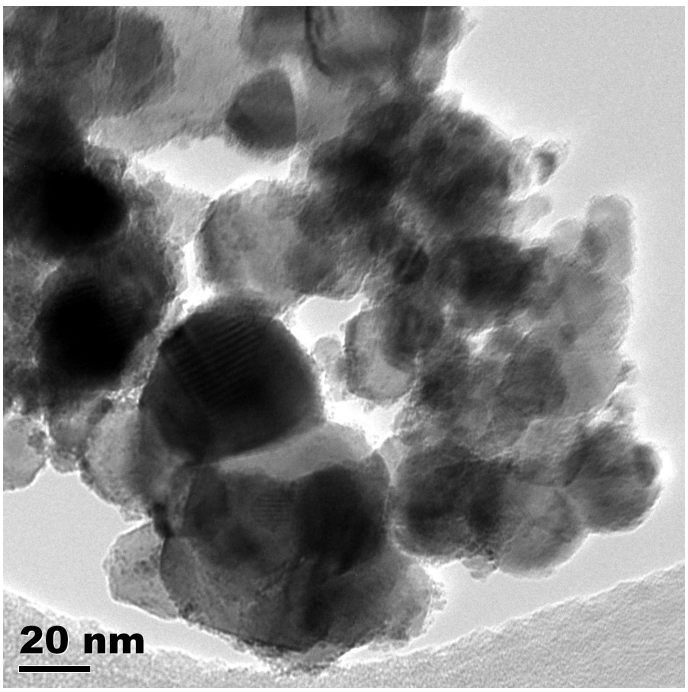

(a) TEM picture of catalyst C177: ATO-$Ru_{0.77}Ta_{0.23}O_2$ at 100k times magnification. The catalyst particles can be seen as small dots. The larger particles (>20nm) are ATO particles.

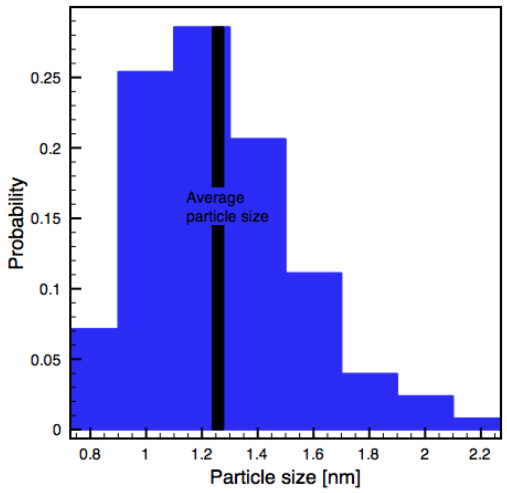

(b) Particle size distribution of catalyst C177: ATO-$Ru_{0.77}Ta_{0.23}O_2$

Figure 4.4: TEM picture and particle size distribution of catalyst C177.

4.3 Synthesis variation: 4h reduction at 190°C

Achieving a high tantalum composition in the catalysts proved to be difficult. As table 4.1 showed in the beginning of this chapter, the attempt of getting 20 and 40at% Ta resulted in 4 and 23at% respectively. As explained in section 2.3, the reduction of the metal precursors is thermodynamically dependent on temperature. In order to achieve a higher Ta composition, the reduction step temperature was increased to 190°C and the time to 4 hours, but this did not have a signifacant effect. A target of 40at% resulted in 16.7at%, lower than the result from the same aim in the normal reduction step. Catalyst C177, ATO-$Ru_{0.77}Ta_{0,23}O_2$, is presented again as a reference in this section as it has the same nominal composition: ATO-$Ru_{0.6}Ta_{0.4}O_2$.

Table 4.4: Normalization factors; catalyst mass applied to the electrode, $m_{catalyst}$ and the positive charge in the CV at 300mV/s, q_{300}.

Synthesis lable	at% Ta	$m_{catalyst}$	q_{300}
C177	23.4at%	$3.53\mu g$	1.263mC
C179 supported	16.7at%	$4.79\mu g$	1.382mC
C179 unsupported	10.3at%	$5\mu g$	0.732mC

The relation between peak current and sweep rate in figure 4.5a is linear, meaning that diffusion is not important. The voltammograms in figure 4.5b have a similar shape as in figure **??**, but the unsupported catalyst showes less distinct peaks than the supported catalysts. Unnormalized cyclic voltammograms are given in appendix B.

The polarization curves in figure 4.6 are normalized with respect to the mass of applied catalyst metal. In the supported catalyst reduced at 190°C for 4h, the "shoulder" at 1.49V has grown to a second peak (region 2). The first peak is located at the same potential as the reference. The unsupported catalyst reduced in the same reduction step (190°C, 4h) have only the second peak, meaning that the catalyst is stable at higher potentials than the supported catalysts. In the linear region of the polarization curves, the unsupported catalyst show a much lower current per unit of applied mass. This indicates that the particles are larger in the unsupported catalyst. TEM-images and particle size distributions are given in figure 4.7.

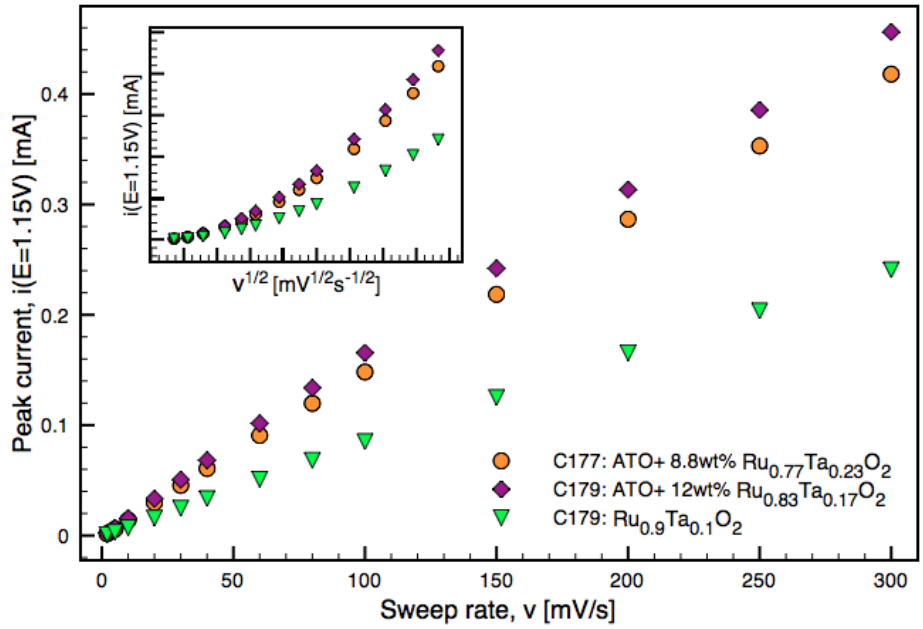

(a) Peak current, I_p, plotted against sweep rate, ν. The subplot shows I_p as a function of $\sqrt{\nu}$.

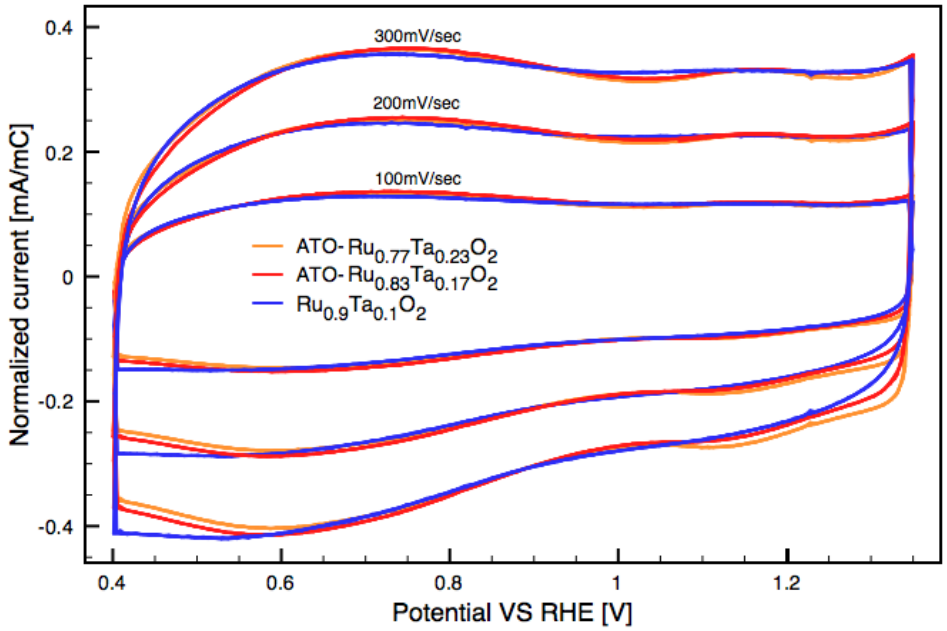

(b) Cyclic voltammograms recorded at 100, 200 and 300 mV/s. The current is normalized with respect to the charge at 300mV/s, q_{300}.

Figure 4.5: Summary of data obtained by cyclic voltammetry.

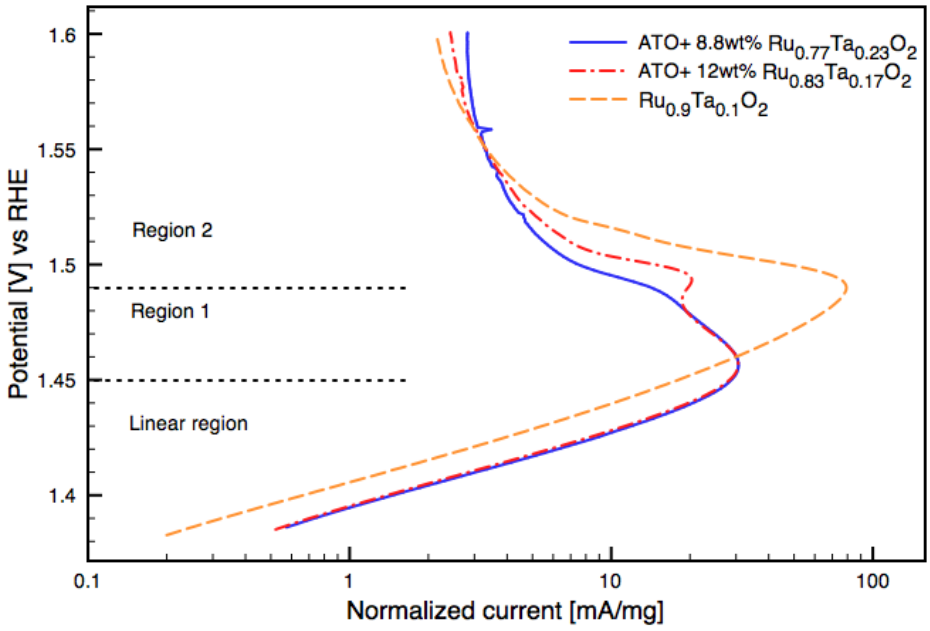

Figure 4.6: Polarization curves normalized with respect to the catalyst mass applied to the electrode. The curves are divided into a linear region, region 1 (1.45V-1.49V) and region 2 (>1.49V).

Table 4.5: Relevant values in the comparison of ATO-$Ru_{1-x}Ta_xO_2$ catalysts.

Catalyst	E_{peak}	Tafel slope	Mean particle size
ATO-$Ru_{0.77}Ta_{0.23O_2}$	1.456V	31.6 mV/dec	1.26nm
ATO-$Ru_{0.83}Ta_{0.17}O_2$	1.457V	32.1 mV/dec	1.47nm
$Ru_{0.9}Ta_{0.1}O_2$	1.490V	32.2 mV/dec	2.74nm

The average particle size of the unsupported $Ru_{0.9}Ta_{0,1}O_2$ is 2.74nm, considerably larger than for the supported catalyst from the same reduction step: 1.47nm. This can not directly be associated with the effect of the catalyst support, but rather with difficulties related to sedimentation of nano sized particles. Only 5% of the catalyst mass were collected without the support present, which in other words means that only the largest particles were collected from the suspension. Figure 4.8 show a diffraction image of the unsupported $Ru_{0.9}Ta_{0,1}O_2$ catalyst taken with TEM. The lack of a diffraction pattern means that the unsupported particles are amorphous. Up to this point all the catalysts have shown properties that can be explained with the theory given in chapter 2.6, but amorphous ruthenium oxide is not considered in the electrochemical equilibrium diagram [7] and the theory based on stable and corrosive sites in the rutile structure [8] does not apply to an amorphous phase. It is clear, however, that either a larger particle size or the lack of crystal structure or both have a positive effect on stability. A small summary of the important values in this section is given in table 4.5

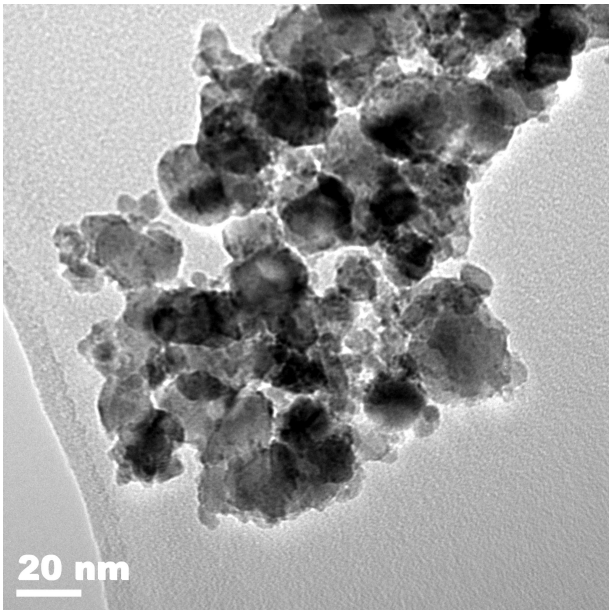

(a) TEM picture of ATO-$Ru_{0.83}Ta_{0.17}O_2$, synthesized with 4h reduction at 190°C. The magnification is 100kX.

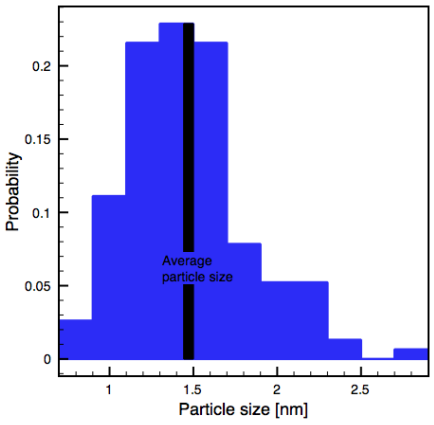

(b) Particle size distribution of catalyst C179-sup.: ATO-$Ru_{0.83}Ta_{0.17}O_2$.

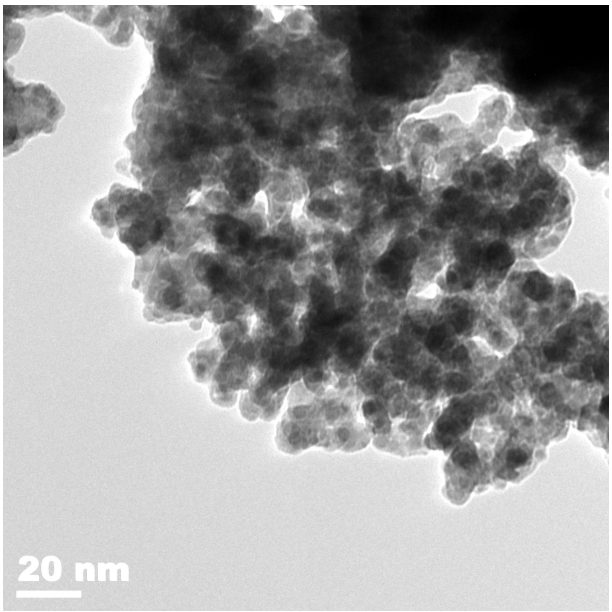

(c) TEM picture of $Ru_{0.9}Ta_{0.1}O_2$, synthesized with 4h reduction at 190°C. The magnification is 100kX.

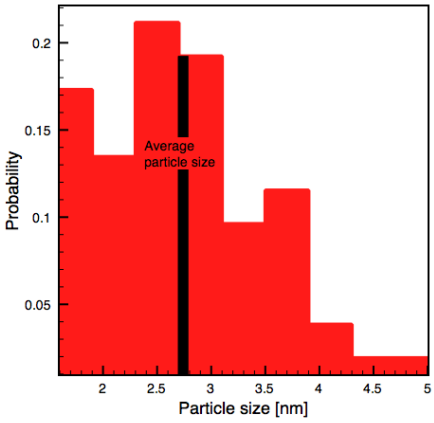

(d) Particle size distribution of catalyst C179-uns.: $Ru_{0.9}Ta_{0.1}O_2$.

Figure 4.7: TEM picture and particle size distribution of catalyst C179, supported and unsupported.

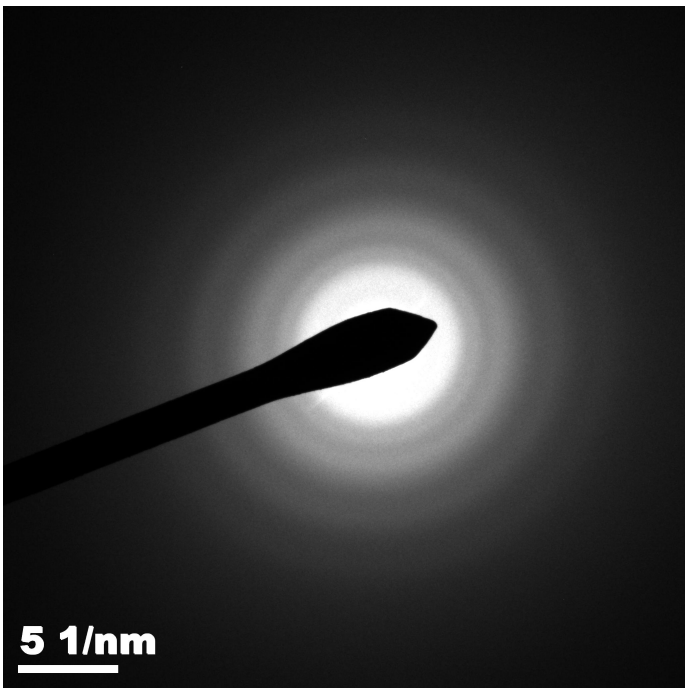

Figure 4.8: No diffraction pattern is observed of unsupported $Ru_{0.9}Ta_{0.1}O_2$, meaning that the catalyst is amorphous. The picture was taken in TEM with 30cm camera constant and 200kV acceleration voltage.

4.4 Synthesis variation: Addition of 10wt% water

Water was added to the EG before reduction of catalyst C180: ATO-RuO_2, with the intention of increasing the catalyst particle size. This catalyst will be compared to C178: ATO-RuO_2, the catalyst synthesized without water present. In figure 4.9a, the peak current is proportional to the sweep rate, and the supported catalysts show voltammograms in figure 4.9b with roughly the same shape as earlier. The peak around 1.15V is almost not detectible in the voltammogram for unsupported ruthenium. The normalization factors are given in table 4.6. Unnormalized cyclic voltammograms are given in appendix B.

The polarization curves in figure 4.10 show that unsupported ruthenium oxide is stable for a longer time than the two supported RuO_2 catalysts. There is a small shift to the left in the linear region of the unsupported RuO_2 curve, indicating that the active area per unit of mass is smaller than for the two supported ruthenium

Table 4.6: Normalization factors; catalyst mass applied to the electrode, $m_{catalyst}$ and the positive charge in the CV at 300mV/s, q_{300}.

Synthesis lable	$m_{catalyst}$	q_{300}
C178	$4.95\mu g$	2.547mC
C180 supported	$5.66\mu g$	2.196mC
C180 unsupported	$5\mu g$	1.128mC

catalysts. Like in section 4.3, this can be the consequence of a larger particle size, but the effect seen in figure 4.10 is smaller than what is observed in the previous section. A small difference in the dissolution potentials is observed in the supported catalysts synthesized with, and without, water. The polarization curves for ATO-RuO_2 follow the same trend in region 1 and 2. TEM images and particle size distributions for catalyst C180 are given in figure 4.11. A summary of the most important values is given in table 4.7.

Table 4.7: Relevant values in the comparison of ATO-RuO_2 catalysts.

Catalyst	E_{peak}	Tafel slope	Mean particle size
C178, ATO-RuO_2	1.451V	31.4 mV/dec	-
C180, ATO-RuO_2	1.451V	31.3 mV/dec	1.35nm
C180, RuO_2	1.464V	30.0 mV/dec	1.76nm

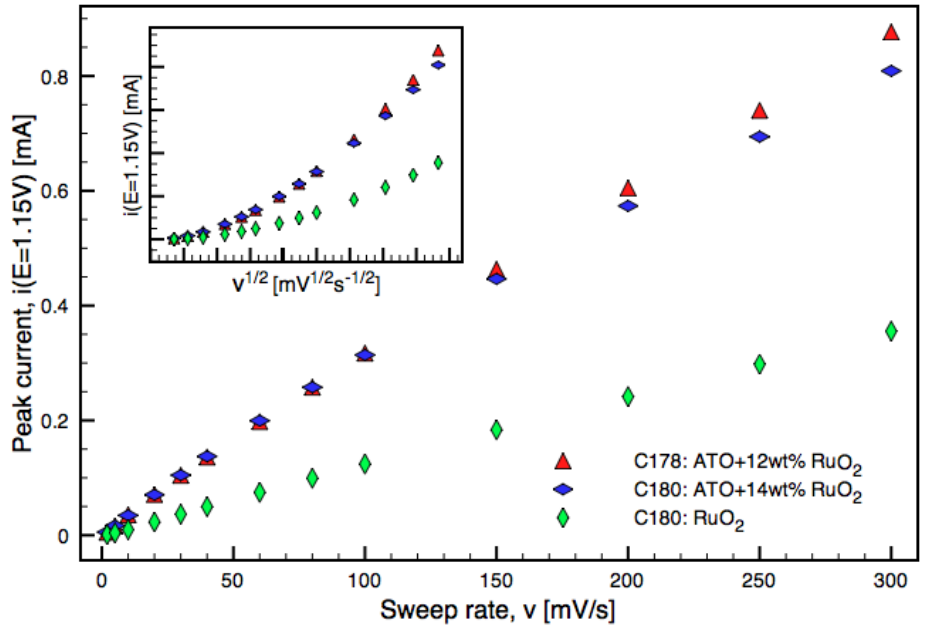

(a) Peak current, I_p, plotted against sweep rate, ν. The subplot shows I_p as a function of $\sqrt{\nu}$.

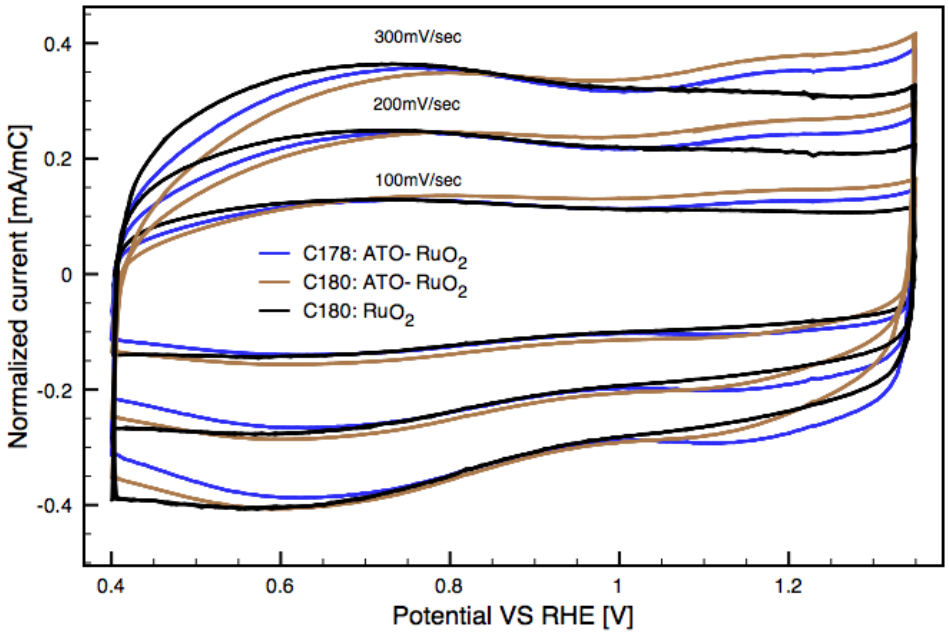

(b) Cyclic voltammograms recorded at 100, 200 and 300 mV/s. The current is normalized with respect to the charge at 300mV/s, q_{300}.

Figure 4.9: Summary of data obtained by cyclic voltammetry.

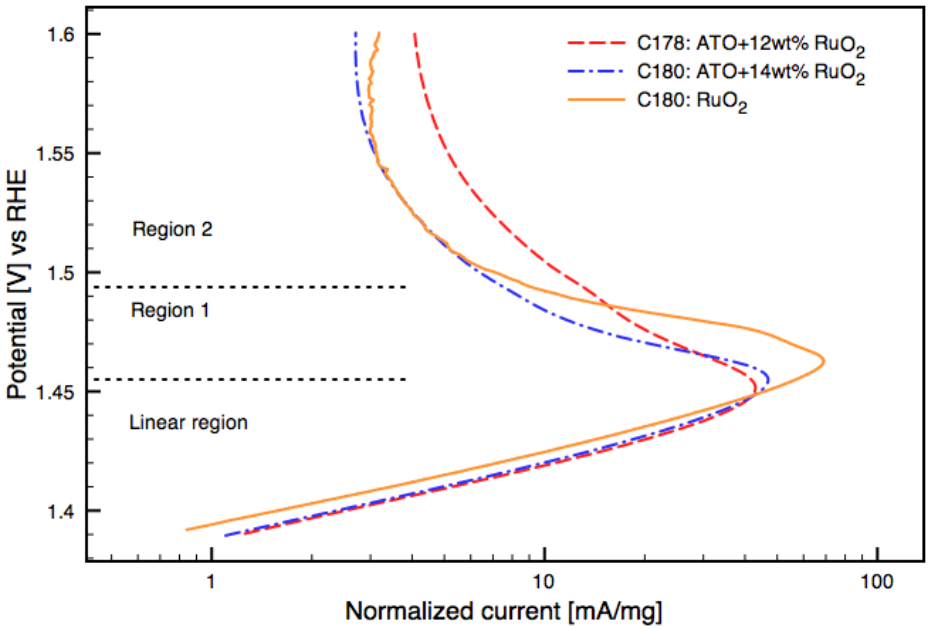

Figure 4.10: Polarization curves normalized with respect to the catalyst mass applied to the electrode.

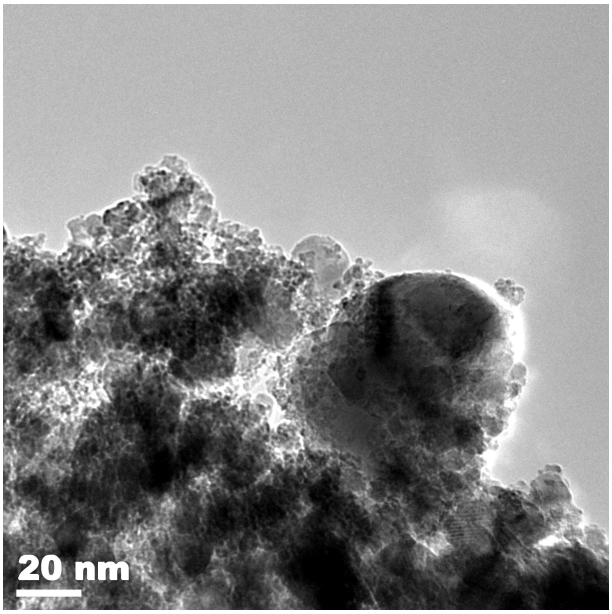

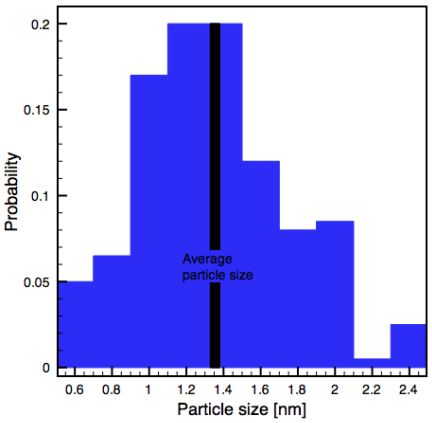

(a) TEM picture of C180: ATO-RuO_2, synthesized with 10wt% water in the EG. The magnification is 100kX.

(b) Particle size distribution of catalyst C180: ATO-RuO_2.

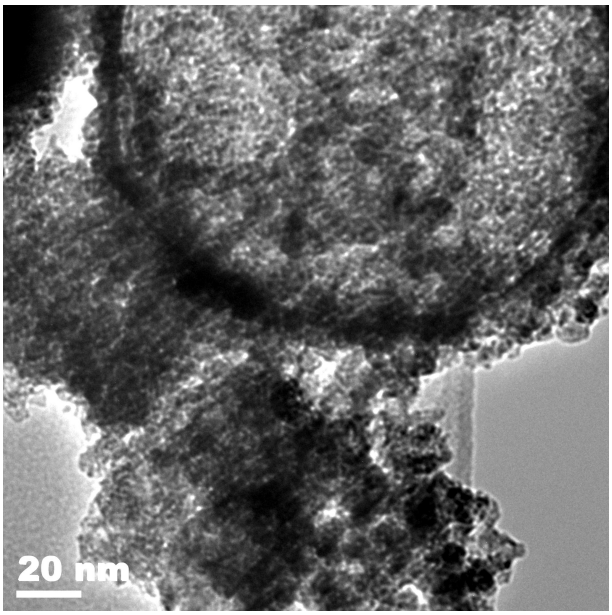

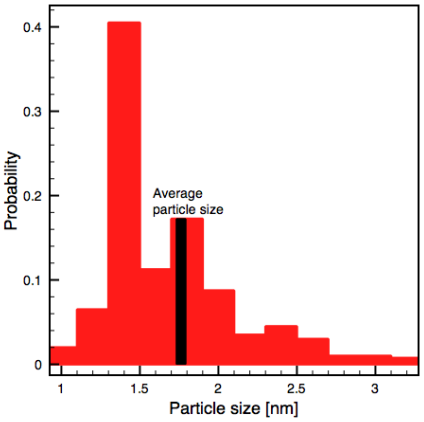

(c) TEM picture of C180: RuO_2, synthesized with 10wt% water in the EG. The magnification is 100kX.

(d) Particle size distribution of catalyst C180: RuO_2.

Figure 4.11: TEM picture and particle size distribution of catalyst C180, supported and unsupported, synthesized in EG and 10wt% water.

Figure 4.12 shows a diffraction pattern of the unsupported RuO_2 catalyst. Unlike the unsupported $Ru_{0.9}Ta_{0.1}O_2$ catalyst presented in section 4.3, this catalyst is crystalline. The RuO_2 particle size is also smaller than the $Ru_{0.9}Ta_{0.1}O_2$ catalyst, which means that more of the catalyst was successfully removed from the EG suspension.

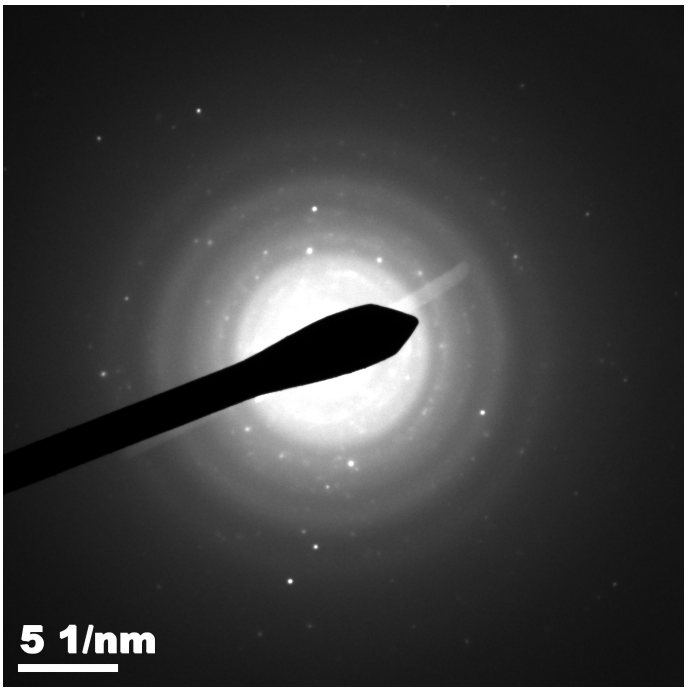

Figure 4.12: Diffraction pattern of unsupported C180: RuO_2 with 30cm camera constant and 200kV accelerating voltage.

4.5 Summarizing results

The dissolution potentials are plotted against Ta composition and particle size in figure 4.13. Figure 4.13a show that when tantalum is present, the peak potential is slightly higher, indicating that the stability is slightly improved. Figure 4.13b however shows a significant stabilizing effect of particle size. It is important to note that these figures neglect all parameters but the one plotted on the x-axis. This means that while figure 4.13a shows an effect of tantalum, this is neglected in figure 4.13b, and vice versa.

Because the peaks in the polarization curves happen around 1.455V, this potential was chosen for the chronoamperometric study. Figure 4.14 show the measured current plotted against time in a log-log relation. The polarization curves have previously shown that C179uns, $Ru_{0.9}Ta_{0.1}O_2$ has the highest stability but the catalytic activity is lowered when tantalum is present. This can also be seen in figure 4.14.

From figure 4.14, lifetime can be defined as the time it takes for the current to reach 10% and 50% of the initial current. The initial current is set to the current 10 seconds after the potential step. To illustrate, the chronoamperometric curves, normalized with respect to the initial current are given in appendix C. In figure 4.15, lifetime is plotted versus different parameters. The 10% line in figure 4.15a show an almost linear relation between the logarithm of lifetime and particle size. In the 50% line, C179sup: ATO-$Ru_{0.83}Ta_{0.17}O_2$ gets a lower lifetime than C180sup: ATO-RuO_2, even though the polarization curves show that the dissolution potential is increased when tantalum is present. In figure 4.15b the same lifetimes are plotted against the positive charge in the CV at 300mV/s divided by the mass applied to the electrode, $q_{300}/m_{catalyst}$. This parameter can be seen as the amount of active mass, or volume, per unit of applied mass, and is related to the particle size. Figure 4.15c shows the relation between the lifetime ($t(I = 0.1I_{initial})$ and the catalytic activity, measured as the current at 1.42V in the polarization curves. This figure show that the catalysts with low activity have a higher stability, and that tantalum is reducing the catalytic activity.

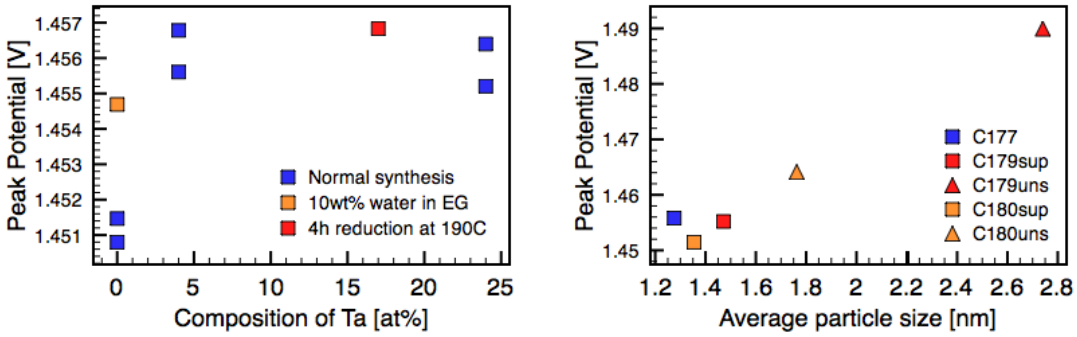

(a) Peak potential versus Ta-composition. (b) Peak potential versus average particle size.

Figure 4.13: Peak potential plotted against Ta composition and particle size.

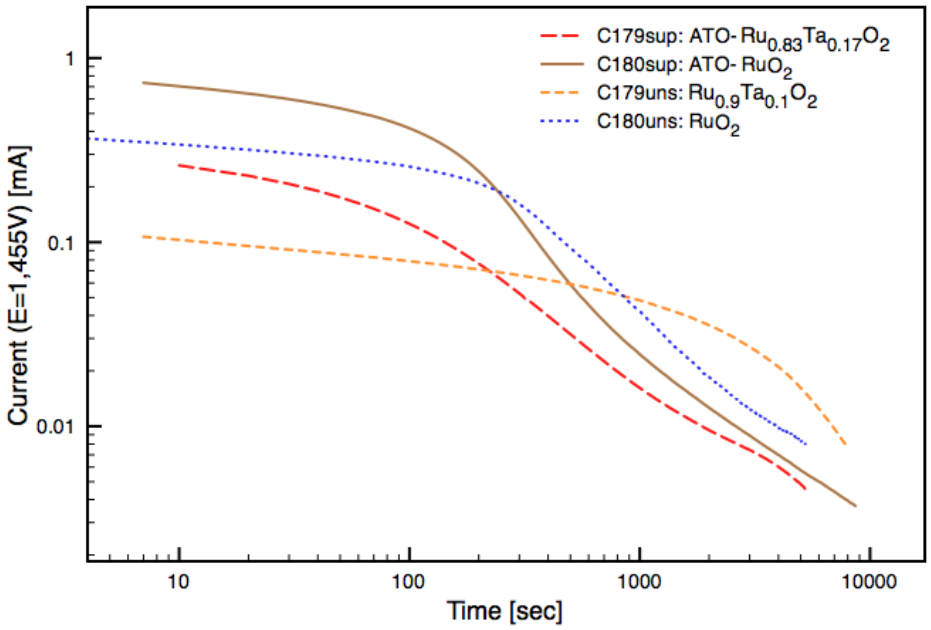

Figure 4.14: Chronoamperometric study of C179 and C180. Measured current at 1.455V as a function of time.

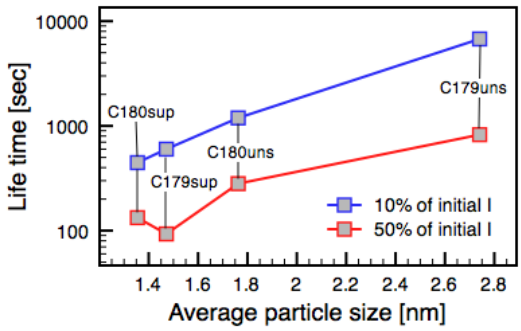

(a) Life time, $t(I = 0.1I_{initial})$ and $t(I = 0.5I_{initial})$, versus particle size.

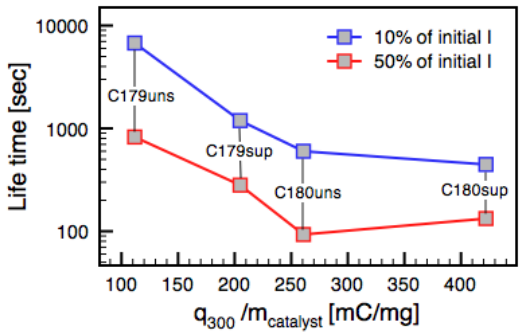

(b) Life time, $t(I = 0.1I_{initial})$ and $t(I = 0.5I_{initial})$, versus $q_{300}/m_{catalyst}$.

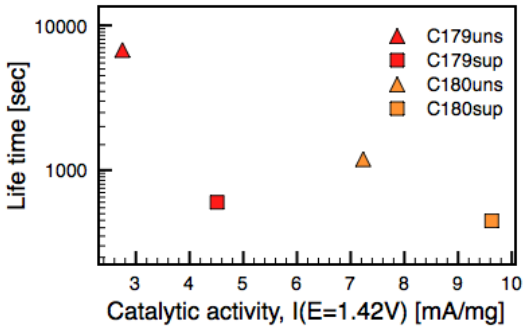

(c) Life time, $t(I = 0.1I_{initial})$, versus the catalytic activity, seen as the current at 1.42V in the polarization curves normalized with respect to the mass applied to the electrode.

Figure 4.15: Life time plotted against different parameters for the supported and unsupported catalysts labeled C179 and C180.

5 Discussion

5.1 The polyol synthesis method

The polyol synthesis method is quite stable, even though the parameters in the reduction step were intentionally changed. In this work, increasing the catalyst particle size was attempted with the addition of water. Increasing the tantalum composition was attempted by applying longer reduction time at a higher temperature. Neither of these measures resulted in the desired effect.

Getting a catalyst loading of 20wt% proved to be difficult in all the catalysts but the first. C176 resulted in good deposition of the catalyst particles since 20wt% loading was obtained. The supernatant after centrifugation had a transparent yellow color, which is a sign of a high yield. In this synthesis the tantalum composition was just around 25% of what was expected, and since tantalum weighs more than ruthenium, this should have had an effect on the loading. However, some ATO did not disperse properly before the deposition step in C176, leading to lost ATO and increased loading. When 40at% tantalum was added in the second synthesis, C177, the supernatant was still transparent, but now the yield and loading were much lower than what was expected. The Ta composition was increased but it was still only 23at%. It is fair to assume that difficulties associated with reduction of $TaCl_5$ are the main cause. The molar weight of Ta is close to twice the molar weight of Ru, and less reduced tantalum leads to a poor loading and a poor yield. The supported RuO_2 catalyst, C178, achieved a higher loading than C177, but not as high at 20wt%. It should be expected that the deposition on ATO slows down, as less free surface area of the ATO particles remains available. 20wt% of pure ruthenium has a larger volume than 20wt% of $Ru_{0.8}Ta_{0.2}O_2$ because of the lower molar mass. This implies that a supported RuO_2 catalyst will get a lower loading than a heavier catalyst. This is however only speculations since the coverage on ATO has not been investigated in this work. C179 and C180 both show the same trend as C177 and C178 with respect to the loading. The high loading in C176 is assumed to be the consequence of lost ATO during the preparation of the ATO dispersion.

The particle size of the supported catalysts, C177, C179 and C180 are surprisingly similar with just 0.25nm difference between the smallest and the largest average. C179, which was reduced at 190°C, should by the arguments posed in section 2.3 [16] get the highest number of nuclei and thus the smallest particle size. However, C179 resulted in an average particle size close to 1.5nm. In other words: C179 got a larger particles than the catalyst who was designed to have the largest particle size, C180. The extra hour at the reduction temperature may have been the cause

of the bigger particles. To set it into perspective: there was clearly no practical effect of the two variations with respect to the average particle size in the supported catalysts. The two unsupported catalysts did get a larger particle size, but not because of the reduction step. This was a consequence of incomplete sedimentation of the catalyst particles. Since larger particles are more easily extracted from dispersion, the centrifugation acts like a filter by giving sedimentation of only the particles above a given size. $Ru_{0.9}Ta_{0.1}O_2$ was centrifuged and washed directly after the reduction step, while RuO_2 was left for a long time to agglomerate before centrifugation. This can explain why $Ru_{0.9}Ta_{0.1}O_2$ got a larger particle size than RuO_2.

In C180, 10wt% water was added to the synthesis. This was supposed to reduce the concentration of acetaldehyde, decreasing the number of nuclei and increasing the particle size by the arguments presented in section 2.3. The water content should also have reduced the concentration of glycolate, according to reaction (2.6). However, a much larger buffer capacity was observed in this synthesis around pH1.5, indicating that there was in fact more glycolate, or possibly some other organic acid, present. In any case, it seems that complete deposition is not possible at a pH above the buffer zone. This means that there is at least one surfactant in the EG after reduction, and the surfactant is removed when the pH is lowered.

5.2 Catalytic activity

It is clear that tantalum additions reduce the catalytic activity. It can be seen from both the polarization curves and from the positive charge in the voltammograms recorded at 300mV/s. When tantalum is present, the charge at 300mV/s divided by the unit of applied mass drops. This can be seen from the polarization curves as the linear part is shifted to the left when the current is normalized with respect to mass in figure 4.3b, while the catalytic activities are the same when the current is normalized with respect to the charge in figure 4.3a. The Tafel slope stays practically the same with the exception of pure unsupported ruthenium oxide. While the other catalysts have a Tafel slope of 31-32mV/dec, C180uns has a Tafel slope of 30.0mV/dec. This might indicate that to some extent, the oxygen evolution reaction is slowed down by both the support and the additions of tantalum. The values are consistent with other reported data for ruthenium oxide [25]. A Tafel slope of 30mV/dec suggest that reaction (2.10) listed in section 2.4.2 is the rate determining mechanism in the system.

5.3 Catalyst stability

5.3.1 Effect of tantalum

The dissolution potential for ruthenium is slightly increased with the addition of only 4at% tantalum. However, the potential is not further increased when another 20at% is added. Since the potential only increases around 5 mV, and the dissolution potential is still far below what is demanded in a practical application, stabilization by tantalum additions will have to be regarded as ineffective, for the kind of catalysts investigated in this work. The 5mV increase can have a purely thermodynamic reason, as the oxidation potential would increase as the activity of the reactant is lowered. The supported catalysts containing tantalum have a drop in current at about 1.49V in the polarization curves. The drop in current is not observed in the pure ruthenium catalysts, at least not to the same extent. This indicates that the catalyst degradation is accelerated above 1.49V when tantalum is present. One possible mechanism might be that tantalum is dissolved, much like ruthenium. Another might be that the tantalum locates itself on the stable crystal sites and pushes ruthenium to the corrosive sites, oppositely of how iridium behaves.

In the supported catalyst reduced at 190°C for 4 hours, C179sup, there is a second peak at around 1.49V. In the same potential region, the unsupported product from this synthesis has its only current peak. Additionally, the unsupported $Ru_{0.9}Ta_{0.1}O_2$, C179uns, was shown to be amorphous, while the unsupported RuO_2 catalyst, C180uns, was shown to have a crystal lattice. These results suggest that the second peak correspond to an amorphous phase since only C179 had both. The tantalum composition in the two C179 catalysts was lower than in C177. The second peak could therefore not be an effect of tantalum alone. In this case the combination of increased time and temperature lead to an amorphous phase, but it is not certain that either will do the same individually. Assuming that the second peak correspond to degradation of amorphous $Ru_{1-x}Ta_xO_2$, the synthesis could be manipulated in order to get more or less of the amorphous phase, resulting in a larger or smaller peak at 1.49V compared to the one at 1.455V. It may well be that tantalum plays an important role in determining the phase composition because a crystal lattice was present in the unsupported RuO_2 catalyst, and not in the unsupported $Ru_{0.9}Ta_{0.1}O_2$ catalyst.

In total, tantalum seems to have more negative effects than positive. It lowers the activity and seems to destabilize ruthenium above 1.49V. However, if tantalum stabilizes an amorphous phase with ruthenium and the stability of this phase is dependent on the composition of tantalum, this could be a way to make a stable

oxygen evolution catalyst without relying on expensive iridium.

5.3.2 Effect of particle size

The figures showing stability plotted versus particle size (figures 4.13b and 4.15a) are both assuming that none of the other factors have an effect on stability. Because most of the catalysts have different synthesis routes or compositions, this is a bold assumption. The effect of particle size can therefore be seen from catalyst C180, supported and unsupported. These catalysts are pure ruthenium oxide with a 0.4nm difference in average particle size. With this increase in particle size the dissolution potential was increased with 13mV, and the lifetime was increased from 446 to 1191 seconds (lifetime defined as $t(I = 0.1I_{initial})$ at 1.455V vs RHE). In the stability figures, these two catalysts fit quite well with the other data points in an increasing trend. There is, however, one factor that is not considered here: the effect of ATO. Unfortunately, a supported and an unsupported catalyst with the same particle size were not obtained in this work, and since the supported catalysts have similar particle sizes and quite different tantalum compositions, there is no way of isolating the individual effect of the support. When all the catalysts are considered it seems that the particle size has a larger impact on stability than the tantalum composition. The catalyst with the largest particles, C179uns, is the most stable one, but it is hard to say if this is due to the particle size, the amorphous phase structure or a combination of both.

5.4 Normalization of current

As explained in section 2.5.1; because of the linear relation between peak current in the voltammograms and the sweep rate, the outer and inner charge cannot be calculated and used as normalization factors. Due to this, the charge in the voltammogram recorded at 300mV/s, q_{300}, was used to normalize the current with respect to the active surface area. As seen in the I_p vs. ν figures the trends are not completely linear for all the catalysts. On the other hand, the trends are not linear in any of the I_p vs. $\sqrt{\nu}$ plots. In spite of this, normalization with respect to q_{300} resulted in polarization curves that overlapped in the linear region, supporting the assumption that the charge is representative for the active surface area.

When the data was normalized with respect to the applied mass, two factors may contribute to errors. Firstly, the catalyst loading was determined by EDS, a method that is recognized as a quasi-quantitative method. Secondly, the catalyst dispersion was assumed to be completely homogenous, meaning that the mass

could be calculated from the volume and the concentration of the dispersion. In the case where catalysts behave differently in dispersion due to material properties, normalization with respect to the calculated mass can lead to a systematic error. It is therefore possible that a catalyst with a low calculated charge per unit of mass, instead had less applied mass than what was calculated. A systematic error in the current normalization would have an impact on the catalytic activity. However, most of the results presented in this work are based on the dissolution potential and the loss of a percentage of current, not the absolute value of the current.

6 Conclusions

Nanosized $Ru_{1-x}Ta_x$ metal particles were synthesized by reduction in EG at 170°C for 3 hours, before deposition on a support of ATO, and electrochemical oxidation. The catalytic activity, dissolution potential of ruthenium and the lifetime of the catalysts have been investigated and compared with respect to the Ta composition (0-23at%) and particle size (1.25-1.5nm).

Increasing the reduction temperature to 190°C and the reduction time to 4 hours do not increase the Ta composition in the $Ru_{1-x}Ta_xO_2$ particles. However, the catalyst from this synthesis got a fraction of large (2.74nm) amorphous particles with 10at% Ta. These were the most stable particles obtained in this work. To increase the particle size in ATO-RuO_2, 10wt% water was added to the reaction medium before reduction. This had no significant effect on the particle size (1.35nm).

A larger particle size has a positive effect on stability. A 0.4nm increased particle size of RuO_2 leads to an increase of lifetime from 446 to 1191 seconds, when lifetime is defined as $t(I = 0.1I_{initial})$ at 1.455V vs. RHE. To synthesize a catalyst with a large particle size proved to be difficult. The larger catalyst particles were obtained by sedimentation of unsupported catalyst particles. The small particles remained stable in dispersion while the large particles were collected. Because a supported catalyst with a large particle size was not successfully synthesized, it was not possible to isolate the effect of the ATO-support on the stability.

Tantalum additions decreases the catalytic activity significantly. By normalization of the polarization curves, it was shown that tantalum reduces the active surface area equally much whether the composition is 4at% or 23at% Ta.

Tantalum does not stabilize ruthenium like iridium does. A small increase of 5mV in the dissolution potential for ruthenium was observed in the catalysts with 4at% and 23% tantalum. In other words, the dissolution potential does not increase further when the composition of tantalum is increased. It was also observed that the current drops more quickly above 1.49V when tantalum is present in the catalyst. This might suggest that tantalum is destabilizing ruthenium at potentials above 1.49V.

7 Further work

The polyol synthesis method combined with ATO has proven to be so stable with respect to particle size, that changing synthesis parameters has practically no effect. To further investigate the $Ru - Ta$ system with this synthesis route, a stronger reducing agent could be used to see if this has an effect on the tantalum composition. It would be interesting to see if this resulted in a larger amount of the amorphous $Ru_{1-x}Ta_xO_2$ phase, and if this improves the stability of the catalyst.

To get a better idea about the current normalization methods, the mass of catalyst applied to the electrode should be controlled. This can be done by placing many drops of catalyst dispersion on a quartz plate, dry off the liquid and weigh the plate on a scale. In this way, the deviation from the calculated catalyst mass can be determined, and a more accurate normalization with respect to mass can be obtained.

References

[1] A. Marshall, *Electrocatalysts for the oxygen evolution electrode in water electrolysers using proton exchange membranes : synthesis and characterisation.* PhD thesis, Norwegian University of Science and Technology, Faculty of Natural Sciences and Technology, 2005.

[2] P. Millet, F. Andolfatto, and R. Durand, "Design and performance of a solid polymer electrolyte water electrolyzer," *International Journal of Hydrogen Energy*, vol. 21, no. 2, pp. 87 – 93, 1996.

[3] E. Rasten, G. Hagen, and R. Tunold, "Electrocatalysis in water electrolysis with solid polymer electrolyte," *Electrochimica Acta*, vol. 48, no. 25-26, pp. 3945 – 3952, 2003.

[4] E. Antolini and E. Gonzalez, "Ceramic materials as supports for low-temperature fuel cell catalysts," *Solid State Ionics*, vol. 180, no. 9-10, pp. 746 – 763, 2009.

[5] S. Trasatti, "Electrocatalysis in the anodic evolution of oxygen and chlorine," *Electrochimica acta*, vol. 29, no. 11, pp. 1503–1512, 1984.

[6] R. Kötz and S. Stucki, "Stabilization of RuO2 by IrO2 for anodic oxygen evolution in acid media," *Electrochimica acta*, vol. 31, no. 10, pp. 1311–1316, 1986.

[7] M. Pourbaix, *Atlas of Electrochemical Equilibria.* Pergamon press, 1966.

[8] I. Man, *Theoretical study of Electro-catalysts for oxygen evolution.* PhD thesis, 2011.

[9] A. Marshall, S. Sunde, M. Tsypkin, and R. Tunold, "Performance of a PEM water electrolysis cell using IrxRuyTazO2 electrocatalysts for the oxygen evolution electrode," *International Journal of Hydrogen Energy*, vol. 32, no. 13, pp. 2320–2324, 2007.

[10] W. C.H. Hamann, A. Hamnett, *Electrochemistry.* Wiley-VCH, 2007.

[11] Frano and Barbir, "PEM electrolysis for production of hydrogen from renewable energy sources," *Solar Energy*, vol. 78, no. 5, pp. 661 – 669, 2005.

[12] J. Bockris, "Kinetics of activation controlled consecutive electrochemical reactions: anodic evolution of oxygen," *The Journal of Chemical Physics*, vol. 24, p. 817, 1956.

[13] Y. Matsumoto and E. Sato, "Electrocatalytic properties of transition metal oxides for oxygen evolution reaction," *Materials Chemistry and Physics*, vol. 14, no. 5, pp. 397 – 426, 1986.

[14] C. Bock, C. Paquet, M. Couillard, G. A. Botton, and B. R. MacDougall, "Size-selected synthesis of PtRu nano-catalysts: Reaction and size control mechanism," *Journal of the American Chemical Society*, vol. 126, no. 25, pp. 8028–8037, 2004. PMID: 15212553.

[15] W. Haynes, ed., *CRC Handbook of Chemistry and Physics*. CRC Press/Taylor and Francis, Boca Raton, FL, 92nd edition, (internet version 2012) ed., 2012.

[16] C. Grolleau, C. Coutanceau, F. Pierre, and J.-M. Leger, "Optimization of a surfactant free polyol method for the synthesis of platinum–cobalt electrocatalysts using taguchi design of experiments," *Journal of Power Sources*, vol. 195, no. 6, pp. 1569 – 1576, 2010.

[17] R. M. J., *Surfactants and Interfacial Phenomena*. Wiley-VCH, 3rd ed., 2004.

[18] D. Pletcher, *Instrumental methods in electrochemistry*. Woodhead Publishing, 2001.

[19] D. Michell, D. Rand, and R. Woods, "A study of ruthenium electrodes by cyclic voltammetry and X-ray emission spectroscopy," *Journal of Electroanalytical Chemistry and Interfacial Electrochemistry*, vol. 89, no. 1, pp. 11 – 27, 1978.

[20] L. Owe, *Characterisation of Iridium Oxides for Acidic Water Electrolysis*. PhD thesis, Norwegian University of Science and Technology, 2011.

[21] L. Burke, O. Murphy, J. O'Neill, and S. Venkatesan, "The oxygen electrode. part 8. oxygen evolution at ruthenium dioxide anodes," *J. Chem. Soc., Faraday Trans. 1*, vol. 73, no. 0, pp. 1659–1671, 1977.

[22] J.-M. Hu, J.-Q. Zhang, and C.-N. Cao, "Oxygen evolution reaction on IrO2-based DSA® type electrodes: kinetics analysis of tafel lines and EIS," *International Journal of Hydrogen Energy*, vol. 29, no. 8, pp. 791 – 797, 2004.

[23] S. Ardizzone, G. Fregonara, and S. Trasatti, ""Inner" and "outer" active surface of RuO2 electrodes," *Electrochimica Acta*, vol. 35, no. 1, pp. 263 – 267, 1990.

[24] J. Wu, X. Z. Yuan, J. J. Martin, H. Wang, J. Zhang, J. Shen, S. Wu, and W. Merida, "A review of PEM fuel cell durability: Degradation mechanisms and mitigation strategies," *Journal of Power Sources*, vol. 184, no. 1, pp. 104 – 119, 2008.

[25] M. Wohlfahrt-Mehrens and J. Heitbaum, "Oxygen evolution on Ru and RuO2 electrodes studied using isotope labelling and on-line mass spectrometry," *Journal of Electroanalytical Chemistry and Interfacial Electrochemistry*, vol. 237, no. 2, pp. 251 – 260, 1987.

A Appendix: EDS

The data obtained with EDS is given below in wt%. The oxygen composition in ATO is found from the composition of Sn and Sb. The loading is then calculated by comparing the catalyst metal composition to the weight of ATO. The metal composition in at% is found be using m_{Ta}=180.9 g/mol and m_{Ru}=101.1g/mol.

Table A.1: Summary of EDS data given i wt%. C176, C177 and C178.

(a) C176, ATO-$Ru_{0.8}Ta_{0.2}O_2$ (nominal)

Statistic	Ru	Sn	Sb	Ta
Max	27.3	71.1	6.09	2.09
Min	21.8	65.83	4.93	1.68
Average	23.2	69.31	5.57	19.3
Standard Deviation	1.93	1.75	0.4	0.12

(b) C177, ATO-$Ru_{0.6}Ta_{0.4}O_2$ (nominal)

Statistic	Ru	Sn	Sb	Ta
Max	7.62	83.74	6.26	4.24
Min	7.06	82.32	4.73	3.66
Average	7.39	83.05	5.53	4.03
Standard Deviation	0.18	0.43	0.45	0.16

(c) C178, ATO-RuO_2

Statistic	Ru	Sn	Sb
Max	17.21	78.89	7.86
Min	14.3	75.28	6.47
Average	15.81	77.14	7.05
Standard Deviation	1.32	1.63	0.42

Table A.2: Summary of EDS data given i wt%. C179 and C180.

(a) C179sup, ATO-$Ru_{0.6}Ta_{0.4}O_2$ (nominal)

Statistic	Ru	Sn	Sb	Ta
Max	20.74	82.57	6.13	5.69
Min	8.02	67.62	4.5	2.49
Average	11.3	79.1	5.54	4.05
Standard Deviation	4.59	4.99	0.44	0.81

(b) C179uns, $Ru_{0.6}Ta_{0.4}O_2$ (nominal)

Statistic	Ru	Ta
Max	85.56	21.18
Min	78.82	14.44
Average	82.9	17.1
Standard Deviation	2.21	2.21

(c) C180sup, ATO-RuO_2

Statistic	Ru	Sn	Sb
Max	18.76	76.08	7.94
Min	17.48	74.59	6.26
Average	17.92	75.28	6.8
Standard Deviation	0.41	0.46	0.5

B Appendix: Cyclic Voltammetry

Unnormalized cyclic voltammograms for the catalysts synthesized in this work are given below. The curves correspond to a sweep rate of 100, 200 and 300 mV per second. The normalization factors $m_{catalyst}$ and q_{300} are given in section 4.

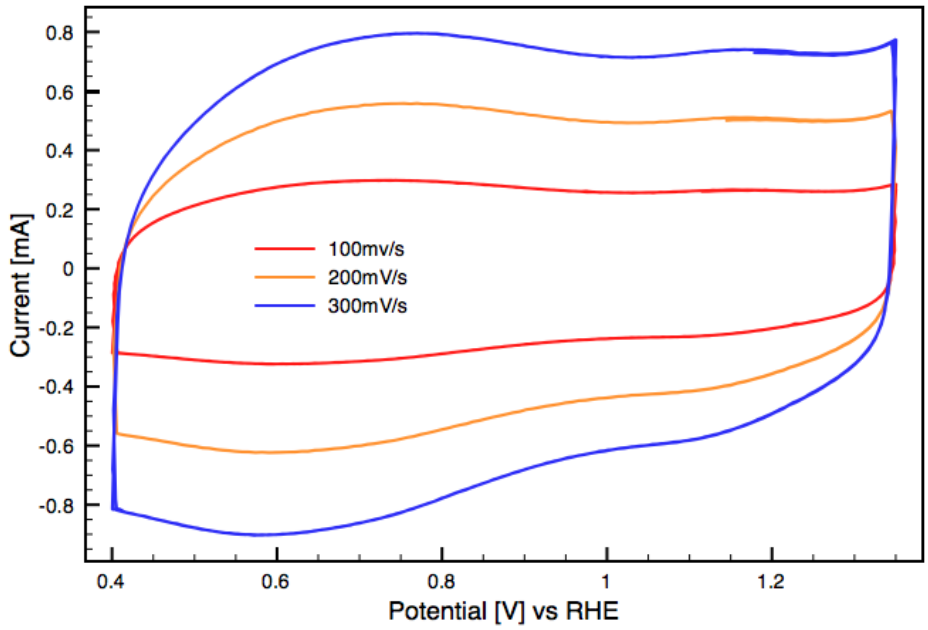

Figure B.1: Unnormalized cyclic voltammetry curves of C176: ATO-$Ru_{0.96}Ta_{0.04}O_2$.

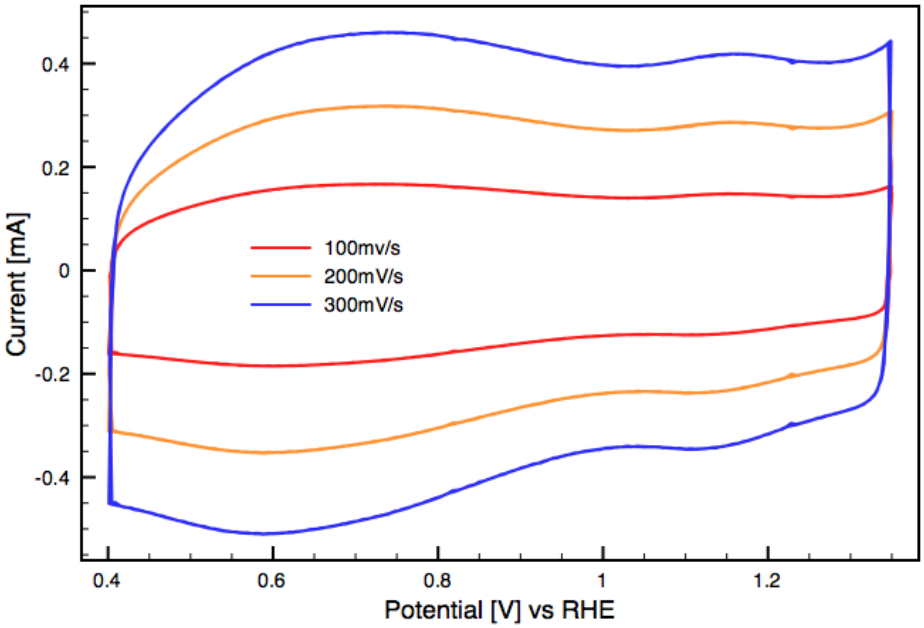

(a) C177: ATO-$Ru_{0.77}Ta_{0.23}O_2$.

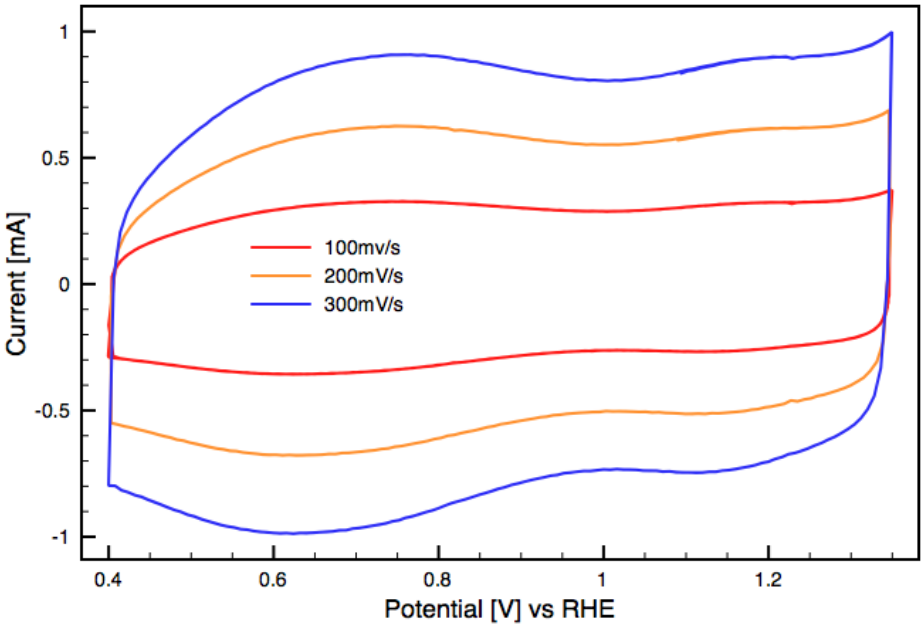

(b) C178: ATO-RuO_2.

Figure B.2: Unnormalized cyclic voltammetry curves of C177 and C178.

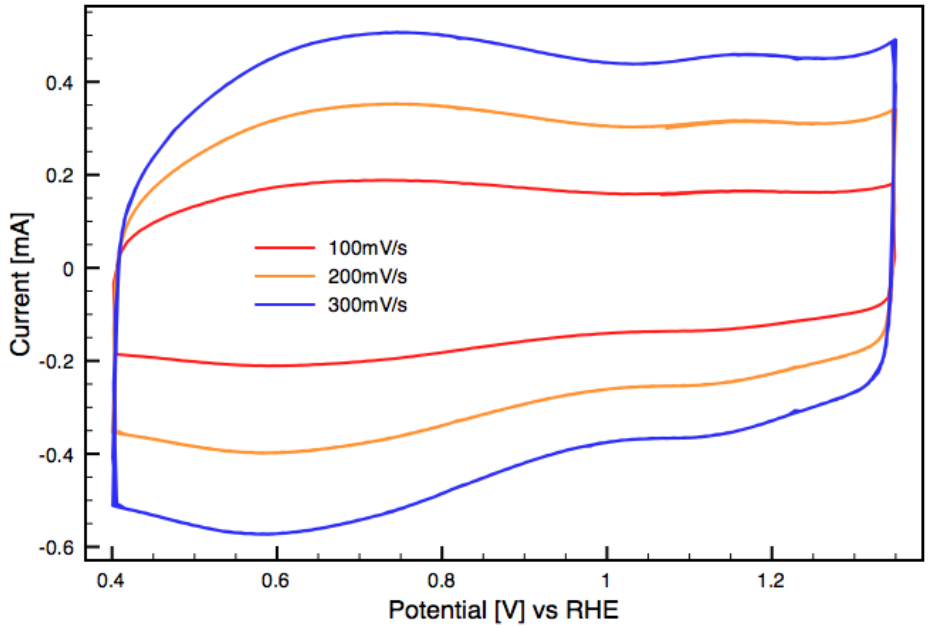

(a) C179sup: ATO-$Ru_{0.83}Ta_{0.17}O_2$.

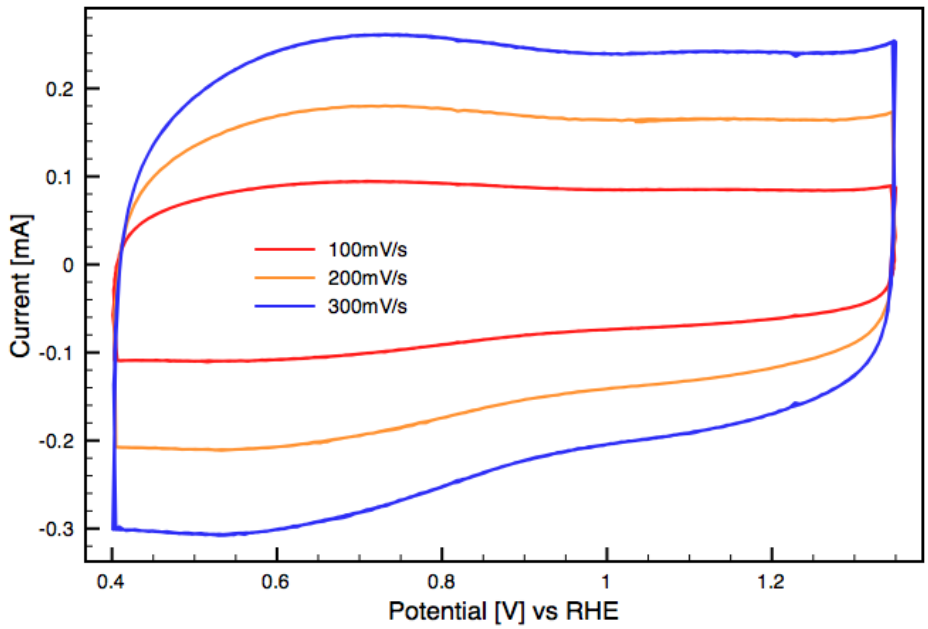

(b) C179uns: $Ru_{0.9}Ta_{0.1}O_2$.

Figure B.3: Unnormalized cyclic voltammetry curves of C179sup and C179uns.

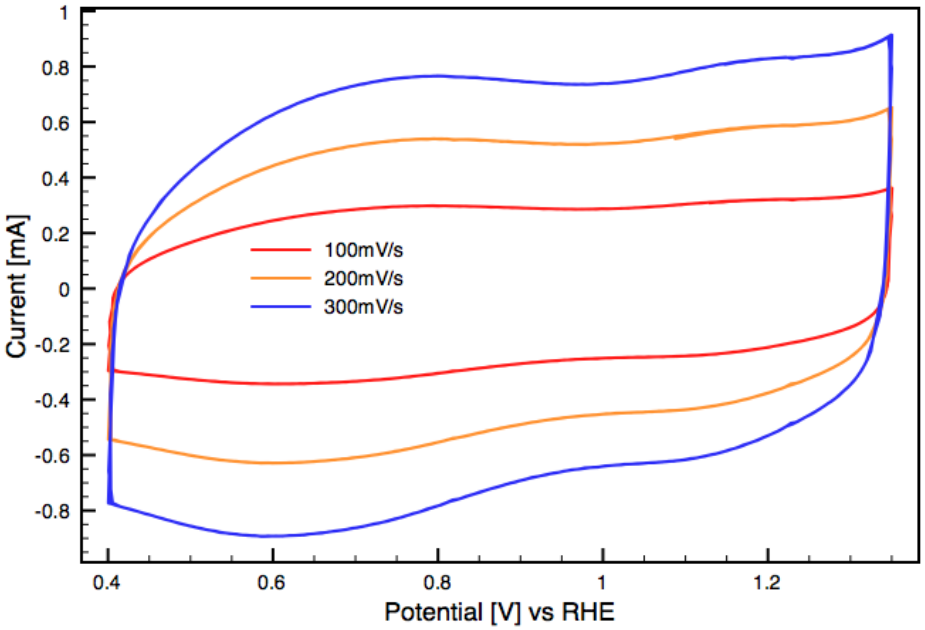

(a) C180sup: ATO-RuO_2.

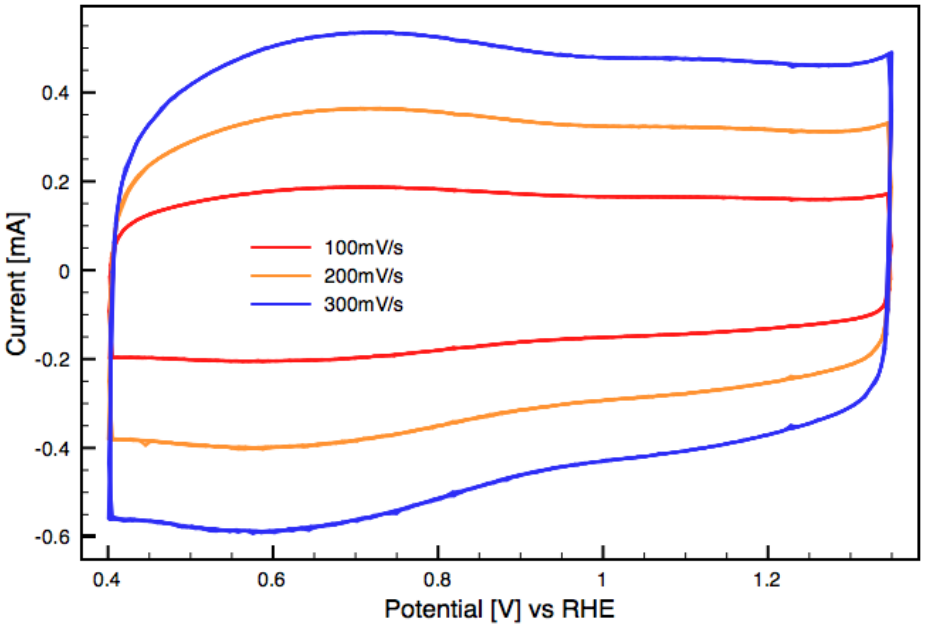

(b) C180uns: RuO_2.

Figure B.4: Unnormalized cyclic voltammetry curves of C180sup and C180uns.

C Appendix: Chronoamperometry

To illustrate the definition of lifetime in this thesis, the figure below show the chronoamperometric curves normalized against the initial current, $I_{initial}$. As mentioned in section 4.5, $I_{initial}$ is defined ad the current 10 seconds after the potential step. The voltage in these experiments were held on 1.455V vs RHE.

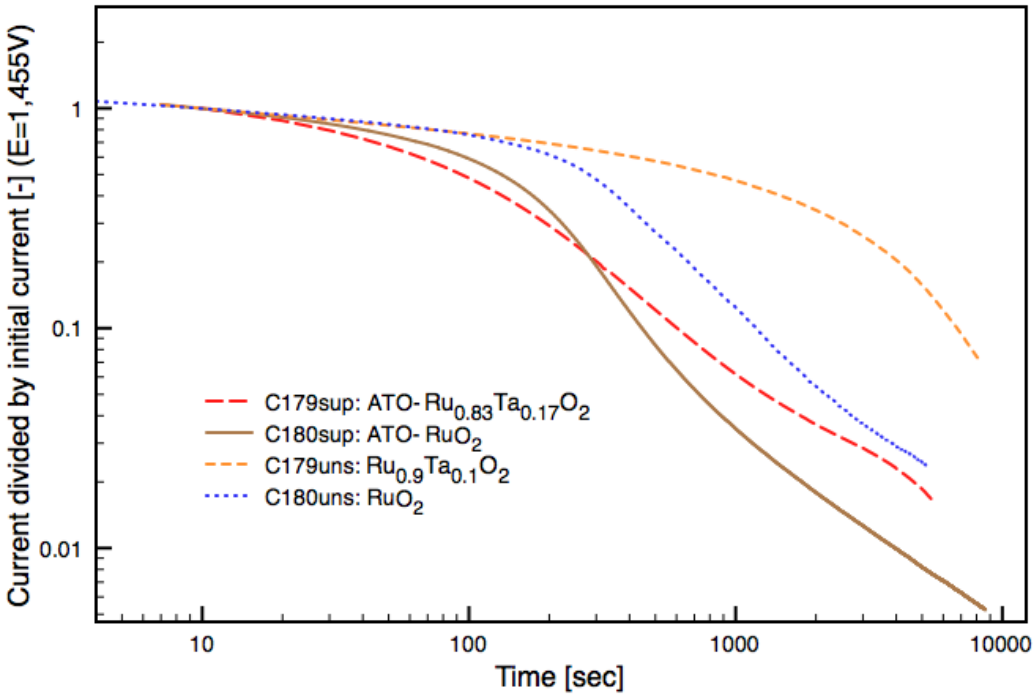

Figure C.1: Chronoamperometric study of C179 and C180. Current, normalized against $I_{initial}$, at 1.455V as a function of time.